nature
structural &
molecular biology

Direct interactions between NEDD8 and ubiquitin E2 conjugating enzymes upregulate cullin-based E3 ligase activity

Eri Sakata[1], Yoshiki Yamaguchi[1], Yasuhiro Miyauchi[2], Kazuhiro Iwai[2], Tomoki Chiba[3], Yasushi Saeki[4], Noriyuki Matsuda[4], Keiji Tanaka[4] & Koichi Kato[1,5]

Although cullin-1 neddylation is crucial for the activation of SCF ubiquitin E3 ligases, the underlying mechanisms for NEDD8-mediated activation of SCF remain unclear. Here we demonstrate by NMR and mutational studies that NEDD8 binds the ubiquitin E2 (UBC4), but not NEDD8 E2 (UBC12). Our data imply that NEDD8 forms an active platform on the SCF complex for selective recruitment of ubiquitin-charged E2s in collaboration with RBX1, and thereby upregulates the E3 activity.

The SKP1/cullin-1/F-box protein (SCF) complex is a multisubunit ubiquitin E3 ligase that promotes ubiquitination of many important regulatory proteins of diverse cellular pathways (see recent review[1]). Cullin-1, together with the RING-finger protein RBX1 (also called ROC1), forms the catalytic core of the SCF complex. The E3 activity of the SCF complex is modulated by the covalent attachment of the ubiquitin-like molecule NEDD8 to cullin-1 (refs. 2–5). This 'neddylation' pathway is considered essential for cell viability in various organisms, though not in budding yeast[3]. In the neddylation process, the APP-BP1–UBA3 heterodimer (NEDD8 E1) and UBC12 (NEDD8 E2) catalyze the formation of an isopeptide bond between the C-terminal glycine residue of NEDD8 and a lysine residue in the cullin homology domain, whereas the COP9 signalosome catalyzes deneddylation[6]. *In vitro* experiments indicate that cullin-1 neddylation upregulates the E3 activity of the SCF complex and thereby enhances protein ubiquitination[2–5]. Furthermore, it has been shown that this modification is important for the recruitment of E2 to the SCF complex[7,8]. However, the underlying mechanisms of the activation of the SCF complex, through the enhancement of E2 recruitment upon neddylation of cullin-1, remain to be understood. We examined the possible interaction of human NEDD8 with human UBC4, which is an E2 enzyme that catalyzes the formation of polyubiquitin chains upon neddylation of cullin-1 (ref. 7).

^{1}H-^{15}N HSQC spectral analyses of isotopically labeled NEDD8 in the presence and absence of unlabeled UBC4 showed chemical shift perturbations of amide resonances for Thr7, Leu8, Ile44, Ser46, Gly47, Lys48, Gln49, Met50, Val70, Leu71 and Leu73, indicating that NEDD8 interacts with UBC4 through its Ile44 hydrophobic patch (**Fig. 1a**, **Supplementary Fig. 1** and **Supplementary Methods** online). In similar titration experiments using UBC12 instead of UBC4, no

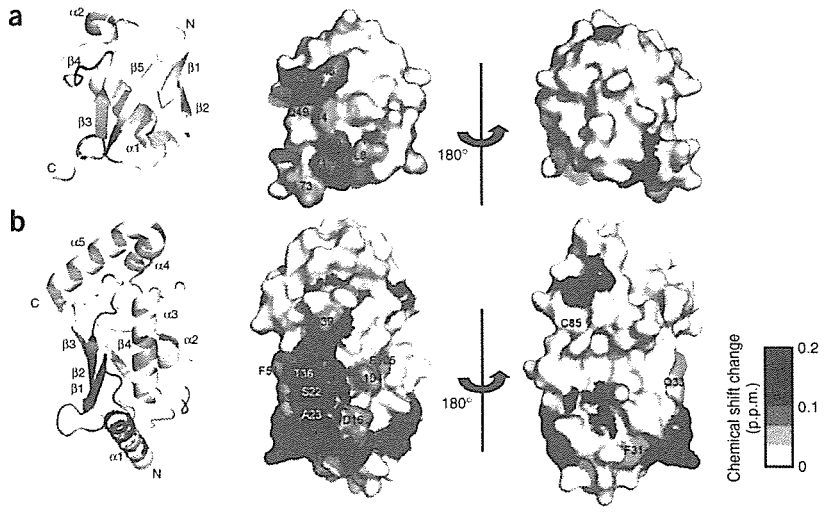

Figure 1 Identification of the binding sites on NEDD8 and UBC4. (**a**,**b**) Mapping of the perturbed residues of NEDD8 (**a**) and UBC4 (**b**) upon binding to each other. Residues are highlighted in red on the crystal structures of NEDD8 (PDB 1NDD) and UBC4 (PDB 2ESK). Red gradient indicates the strength of the perturbation. Blue, residues involved in the interaction with the RING-finger domain in the crystal structure of c-Cbl (PDB 1FBV)[10]; gray, prolines; yellow, catalytic cysteine (C85). This figure was prepared with PyMOL (http://pymol.sourceforge.net).

[1]Department of Structural Biology and Biomolecular Engineering, Graduate School of Pharmaceutical Sciences, Nagoya City University, 3-1 Tanabe-dori, Mizuho-ku, Nagoya 467-8603, Japan. [2]Department of Molecular Cell Biology, Graduate School of Medicine, Osaka City University, 1-4-3 Asahi-machi, Abeno-ku, Osaka 545-8585, Japan. [3]Department of Molecular Biology, Graduate School of Life and Environmental Sciences, University of Tsukuba, 1-1-1 Tennodai, Tsukuba, Ibaraki 305-8577, Japan. [4]Laboratory of Frontier Science, The Tokyo Metropolitan Institute of Medical Science, 3-18-22 Honkomagome, Bunkyo-ku, Tokyo 113-8613, Japan. [5]Institute for Molecular Science, National Institutes of Natural Sciences, 5-1 Higashiyama, Myodaiji, Okazaki, Aichi 444-8787, Japan. Correspondence should be addressed to K.K. (kkato@phar.nagoya-cu.ac.jp).

Received 20 August 2006; accepted 12 December 2006; published online 7 January 2007; doi:10.1038/nsmb1191

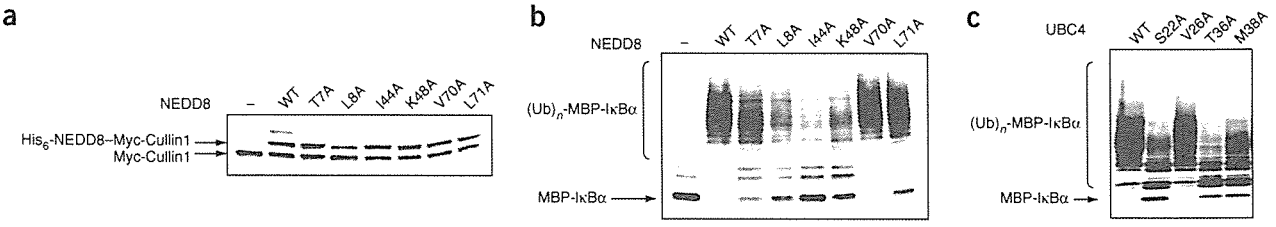

Figure 2 Mutations affecting the NEDD8 and UBC4 interaction compromise upregulation of the E3 activity of $SCF^{\beta\text{-}TrCP1}$ in the ubiquitination of IκBα. (**a**) Effects of NEDD8 mutations on *in vitro* neddylation of cullin-1. (**b**,**c**) Effects of mutations of NEDD8 (**b**) and UBC4 (**c**) on ubiquitination of phosphorylated IκBα. Ubiquitination (symbolized by $(UB)_n$, where *n* represents number of ubiquitins) of a maltose-binding protein (MBP)-IκBα fusion construct by $SCF^{\beta\text{-}TrCP1}$ was examined in the presence or absence of NEDD8 or UBC4 mutants. MBP-IκBα prephosphorylated by IKKβ was used as a substrate.

specific interaction was detected between NEDD8 and UBC12 (**Supplementary Fig. 1**). Next, we identified the NEDD8-binding surface on UBC4. Binding of NEDD8 induced chemical shift perturbations of NMR signals for α1 helix (Leu10, Asp12, Ala14 and Arg15), α1-β1 loop (Asp16, Ala19 and Gln20), β1 strand (Cys20–Ala23), β1-β2 loop (Val26–Phe31) and β2 strand (Trp33–Thr36, Met38 and Gly39) of UBC4 (**Fig. 1b** and **Supplementary Fig. 2** online).

To address the functional relevance of the interaction observed between NEDD8 and UBC4, we mutated the amino acid residues located in the UBC4-binding site of NEDD8 (T7A, L8A, I44A, K48A, V70A and L71A). Whereas these NEDD8 mutants as well as the wild-type NEDD8 were conjugated to cullin-1 to similar extents by *in vitro* neddylation reactions (**Fig. 2a**), an *in vitro* ubiquitination assay revealed differential modulation of their abilities to upregulate the E3 activity of $SCF^{\beta\text{-}TrCP1}$ (substrate-recognition subunit indicated by superscript text) in ubiquitination of IκBα. Notably, the I44A mutant completely lacked the ability to activate this ligase (**Fig. 2b**). An NMR titration experiment confirmed that amino acid substitution of Ile44 with alanine in NEDD8 resulted in loss of its affinity for UBC4 (**Supplementary Fig. 2**). Reciprocally, certain UBC4 mutants with a single amino acid substitution in the NEDD8-binding site (typified by S22A) could not interact with NEDD8 (**Supplementary Fig. 1**) or promote the E3 activity of the neddylated $SCF^{\beta\text{-}TrCP1}$ for ubiquitination of IκBα (**Fig. 2c**), even though these UBC4 mutants had E2 activities comparable to the wild-type UBC4 in *in vitro* ubiquitination reactions with the RMA1 (RING-type) and RSP5 (HECT-type) E3 ligases (**Supplementary Fig. 3** online).

A previous X-ray crystallographic study of SCF^{Skp2} has shown that the neddylation site is in close spatial proximity to the RING-finger domain of RBX1 (ref. 9). The present NMR data suggest that the NEDD8-binding site is distinct from but adjoins the putative RING-binding site on UBC4 (**Fig. 1b**)[10]. On the basis of these data, we propose that NEDD8 provides a hydrophobic surface area for its interaction with the E2 surface area remote from Cys85, the catalytic cysteine, and thereby enhances recruitment of the ubiquitin-charged E2 in collaboration with RBX1. Furthermore, we found that the I44A mutant of NEDD8 did not facilitate the reaction whereby VBC-CUL2 ligase (together with UBCH5c) ubiquitinates its native substrate, indicating that NEDD8-ubiquitin E2 interactions contribute to upregulation of not only cullin-1–based but also cullin-2–based E3 ligase activities (**Supplementary Fig. 4** online).

RBX1 could induce neddylation as well as ubiquitination by allowing alternative binding of different E2s[11]. Our data demonstrate that NEDD8 interacts with the ubiquitin E2, UBC4, but not with the NEDD8 E2, UBC12. The NEDD8-binding sequence in UBC4 identified on the basis of the present NMR data is poorly conserved in UBC12, which explains why UBC12 did not bind NEDD8 (**Supplementary Fig. 5** online). Obviously, ubiquitin and NEDD8 have distinct roles in the proteasome-dependent protein degradation system, despite the fact that these modifiers share 57% amino acid sequence identity. The present study suggests that once NEDD8 is attached onto the cullin subunit, it forms the active platform for selective recruitment of ubiquitin-charged E2 in collaboration with RBX1, excluding the UBC12–NEDD8 complex (**Supplementary Fig. 6** online), and thereby induces substrate ubiquitination. Indeed, cullin-1 neddylation enhances polyubiquitin chain elongation (**Fig. 2b,c**) as well as initial ubiquitin conjugation (**Supplementary Fig. 7** online). The E2-specific interaction of NEDD8 described here could be the mechanism that prevents poly-NEDD8 formation on cullins and concomitantly promotes polyubiquitination of substrates.

Note: Supplementary information is available on the Nature Structural & Molecular Biology website.

ACKNOWLEDGMENTS

We thank T. Kasuya, Y. Kito, K. Senda and K. Hattori for their help in the preparation of recombinant proteins. Work in the laboratory of K.K. and Y.Y. was supported by a Grant-in-Aid for Scientific Research on Priority Areas (17028047 and 18076003) from the Ministry of Education, Culture, Sports, Science and Technology, Japan, and by a Grant-in-Aid for Scientific Research (B) (18390016) from Japan Society for the Promotion of Science. E.S. is a recipient of Japan Society for the Promotion of Science Research Fellowships for Young Scientists.

AUTHOR CONTRIBUTIONS

K.K. contributed to overall guidance of the project. E.S., Y.Y. and K.K. contributed to the design and execution of the NMR study. E.S., K.I., T.C. and K.T. contributed to the design of the mutational studies. E.S., Y.M., Y.S. and N.M. contributed to the execution of the mutational studies. E.S. and K.K. wrote the manuscript. K.I., T.C. and K.T. commented on the manuscript. All authors edited and approved the final version of the manuscript.

COMPETING INTERESTS STATEMENT

The authors declare that they have no competing financial interests.

Published online at http://www.nature.com/nsmb/
Reprints and permissions information is available online at http://npg.nature.com/reprintsandpermissions

1. Petroski, M.D. & Deshaies, R.J. *Nat. Rev. Mol. Cell Biol.* **6**, 9–20 (2005).
2. Kerscher, O., Felberbaum, R. & Hochstrasser, M. *Annu. Rev. Cell Dev. Biol.* **22**, 159–180 (2006).
3. Pan, Z.Q., Kentsis, A., Dias, D.C., Yamoah, K. & Wu, K. *Oncogene* **23**, 1985–1997 (2004).
4. Wu, J.T., Chan, Y.R. & Chien, C.T. *Trends Cell Biol.* **16**, 362–369 (2006).
5. Parry, G. & Estelle, M. *Semin. Cell Dev. Biol.* **15**, 221–229 (2004).
6. Wei, N. & Deng, X.W. *Annu. Rev. Cell Dev. Biol.* **19**, 261–286 (2003).
7. Kawakami, T. *et al. EMBO J.* **20**, 4003–4012 (2001).
8. Wu, K., Chen, A., Tan, P. & Pan, Z.Q. *J. Biol. Chem.* **277**, 516–527 (2002).
9. Zheng, N. *et al. Nature* **416**, 703–709 (2002).
10. Zheng, N., Wang, P., Jeffrey, P.D. & Pavletich, N.P. *Cell* **102**, 533–539 (2000).
11. Megumi, Y. *et al. Genes Cells* **10**, 679–691 (2005).

THE JOURNAL OF BIOLOGICAL CHEMISTRY VOL. 282, NO. 10, pp. 7137–7144, March 9, 2007

A Neural-specific F-box Protein Fbs1 Functions as a Chaperone Suppressing Glycoprotein Aggregation*

Received for publication, December 5, 2006 Published, JBC Papers in Press, January 10, 2007, DOI 10.1074/jbc.M611168200

Yukiko Yoshida[‡§1], **Arisa Murakami**[‡§], **Kazuhiro Iwai**[§¶], **and Keiji Tanaka**[‡]

From the [‡]*Tokyo Metropolitan Institute of Medical Science, 3-18-22 Honkomagome, Bunkyo-ku, Tokyo 113-8613,* [§]*CREST, Japan Science and Technology Corporation (JST), Saitama 332-0012, and the* [¶]*Department of Molecular Cell Biology, Graduate School of Medicine, Osaka City University, 1-4-3 Asahi-cyo, Abeno-ku, Osaka 545-8585, Japan*

Fbs1 is an F-box protein present abundantly in the nervous system. Similar to the ubiquitously expressed Fbs2, Fbs1 recognizes *N*-glycans at the innermost position as a signal for unfolded glycoproteins, probably in the endoplasmic reticulum-associated degradation pathway. Here, we show that the *in vivo* majority of Fbs1 is present as Fbs1-Skp1 heterodimers or Fbs1 monomers but not SCF^{Fbs1} complex. The inefficient SCF complex formation of Fbs1 and the restricted presence of SCF^{Fbs1} bound on the endoplasmic reticulum membrane were due to the short linker sequence between the F-box domain and the sugar-binding domain. *In vitro*, Fbs1 prevented the aggregation of the glycoprotein through the N-terminal unique sequence of Fbs1. Our results suggest that Fbs1 assists clearance of aberrant glycoproteins in neuronal cells by suppressing aggregates formation, independent of ubiquitin ligase activity, and thus functions as a unique chaperone for those proteins.

The SCF (Skp1/Cul1/F-box protein) complex, the largest known class of sophisticated E3[2] ubiquitin ligases, consists of common components, Skp1, Cul1, and Roc1/Rbx1, as well as variable components known as F-box proteins that bind the substrates (1, 2). In this complex, the scaffold protein Cul1 (alias cullin1) interacts at the N terminus with the adaptor subunit Skp1 and at the C terminus with the RING-finger protein Roc1/Rbx1 that recruits a specific ubiquitin-activating enzyme (E2) for ubiquitylation. F-box proteins, interacting with Skp1 through the ~40 amino acid F-box motif, play an indispensable role in the selection of target proteins for degradation because each distinct F-box protein usually binds a protein substrate(s) with a degree of selectivity for ubiquitylation through C-terminal protein-protein interaction domains (3). The human genome contains 69 genes for F-box proteins and a large number of F-box proteins function in the specific ubiquitylation of a wide range of substrates. The F-box proteins are divided into three classes according to the type of substrate-binding domains. The two classes of binding domains are WD40 repeats and leucine-rich repeats, which are named Fbw (or FBXW) and Fbl (or FBXL) families, respectively (4). The third class of F-box proteins is the Fbx (or FBXO) family that does not contain any of these domains.

It has been reported that a subfamily under the Fbx family consists of at least five homologous F-box proteins containing a conserved FBA motif (5, 6). Among them, Fbs1/Fbx2/NFB42/Fbg1 and Fbs2/Fbx6b/Fbg2 can bind to proteins with high mannose oligosaccharides modification that occurs in the endoplasmic reticulum (ER) (7). Experiments using a fully reconstituted system showed that both Fbs1 and Fbs2 can form SCF-type ubiquitin ligase complexes specific for *N*-linked glycoproteins (7, 8). Overexpression of the Fbs1 or Fbs2 dominant-negative form or decrease of endogenous Fbs2 by small interfering RNA resulted in inhibition of degradation of endoplasmic reticulum-associated degradation (ERAD) substrates, suggesting the involvement of SCF^{Fbs1} and SCF^{Fbs2} in the ERAD pathway. Interestingly, x-ray crystallographic and NMR studies of the substrate-binding domain of Fbs1 have revealed that Fbs1 interacts with the innermost chitobiose in *N*-glycans of glycoproteins by a small hydrophobic pocket located at the top of the β-sandwich, indicating that both Fbs1 and Fbs2 efficiently recognize the inner chitobiose structure in $Man_{3-9}GlcNAc_2$ glycans (9). Indeed, the introduction of point mutation into the residues in the pocket impaired the binding activity toward its glycoprotein substrates. In general, the internal chitobiose structure of *N*-glycans in many native glycoproteins is not accessible by macromolecules. Fbs1 interacted with denatured glycoproteins more efficiently than native proteins, indicating that the innermost position of *N*-glycans becomes exposed upon protein denaturation and used as a signal of unfolded glycoproteins to be recognized by Fbs1 (10).

Of the Fbs family proteins, whereas Fbs2 is distributed ubiquitously in a variety of cells and tissues, Fbs1 is expressed only in neurons (7). In considering the involvement of these F-box proteins in the ERAD pathway in general, the restricted expression of Fbs1 in neurons remains a mystery. In this study, we found that the major population of Fbs1 protein did not form the SCF^{Fbs1} complex in cells although Fbs1 is known to act as a compartment of SCF-type ubiquitin ligase (8). Moreover, the results showed that the sequence of the intervening segment between the F-box domain and the substrate-binding domain of the Fbs1 hampered the assembly of the SCF^{Fbs1} complex in the cytosol without affecting the association with Skp1. The Skp1-Fbs1 heterodimers as well as SCF^{Fbs1} complex effectively prevented the aggregation of the glycoprotein *in vitro*, and this

* This work was supported by grants from the Ministry of Education Science and Culture of Japan (to Y. Y. and K. T.). The costs of publication of this article were defrayed in part by the payment of page charges. This article must therefore be hereby marked "*advertisement*" in accordance with 18 U.S.C. Section 1734 solely to indicate this fact.

[1] To whom correspondence should be addressed. Tel.: 81-3-3823-2105; Fax: 81-3-3823-2965; E-mail: yyosida@rinshoken.or.jp.

[2] The abbreviations used are: E3, ubiquitin ligase; ER, endoplasmic reticulum; ERAD, ER-associated degradation; TBS, Tris-buffered saline; RNaseB, ribonuclease B; HA, hemagglutinin.

activity was dependent on the presence of the N-terminal domain and the substrate-binding domain of Fbs1. Our data thus imply that Skp1 and Fbs1 may function in both SCF and non-SCF complexes.

EXPERIMENTAL PROCEDURES

Affinity Purification and Immunoprecipitation of Brain Lysate—The preparation of lysates from mouse brains and purification of Fbs1 by using a ribonuclease B (RNaseB) column were performed as described previously (10). For immunoprecipitation, we used polyclonal antibody to Fbs1 as described previously (11). For immunoblotting, we used rabbit polyclonal antibodies against Fbs1, Cul1 (Zymed Laboratories Inc., San Francisco, CA) and Skp1 (Santa Cruz Biotechnology, Santa Cruz, CA), and horseradish peroxidase-conjugated goat anti-rabbit IgG (Jackson ImmunoResearch Laboratories, West Grove, PA) for Fbs1 and Skp1 blots or horseradish peroxidase-conjugated goat anti-rabbit IgG light chain (Jackson ImmunoResearch Laboratories) for Cul1 blots. Lectin blotting was performed by using horseradish peroxidase-conjugated ConA (Seikagaku-kogyo, Japan) as described previously (11).

Glycerol Gradient Analysis—The fraction eluated with 0.1 M chitobiose from the RNaseB resin was prepared from 0.5 ml of lysates (14 mg/ml) from mouse brains. The eluate was dialyzed against TBS. The resultant fraction and a 1-mg lysate of brains were used for glycerol gradient analysis. Samples and molecular weight markers (Amersham Biosciences) were fractionated by 4–17% (v/v) linear glycerol density gradient centrifugation (22 h, 100,000 × *g*) as described previously (12).

Cell Culture and Immunological Analysis—PC12 cells were grown in RPMI medium 1640 (Invitrogen) supplemented with 10% horse serum and 5% fetal bovine serum. For neuronal differentiation, PC12 cells were treated with 10–20 ng/ml nerve growth factor (Invitrogen) on collagen-coated plates. 293T and HeLa cells were grown in Dulbecco's modified Eagle's medium (Sigma) supplemented with 10% fetal bovine serum and were transfected as described previously (8). FLAG-tagged Fbs1 mutant vectors consisting of Fbs1 and Fbs2 fragments were generated by PCR, and those sequences were verified. Whole cell lysates were prepared with 20 mM Tris-HCl (pH 7.5), 150 mM NaCl (TBS) containing 0.5% Nonidet P-40. The supernatant and precipitate fractions were prepared by ultracentrifugation of the supernatant that was prepared by centrifugation of freezing-and-thawing cell lysates in TBS at 8,000 × *g* for 20 min and at 100,000 × *g* for 60 min. The precipitate fraction was solubilized with Triton X-100. Each immunoprecipitation analysis was performed for whole cell lysates or subcellular fraction of cells by using the same amount of proteins. Monoclonal antibodies to calnexin and rhodopsin were purchased from BD Transduction Laboratories and Affinity Bioreagents (Golden, CO), respectively. Antibodies to FLAG, HA, and fetuin have been described previously (8).

Pulse-chase Analysis—The expression plasmid for P23H rhodopsin was kindly provided by M. E. Cheetham (University College London). Pulse-chase experiments were performed as described previously (7). Briefly, 293T cells were transfected with 1 μg of P23H rhodopsin expression plasmid and 1 μg of FLAG-tagged Fbs1 derivatives or pcDNA3-FLAG plasmid. Twenty-four hours after transfection, the cells were starved for 30 min and labeled for 1 h with 150 μCi of Pro-Mix L-^{35}S *in vitro* cell labeling mix (Amersham Biosciences) per milliliter. After washing, the cells were chased with complete Dulbecco's modified Eagle's medium supplemented with fetal bovine serum in the presence or in the absence of 50 μg/ml MG132 (Peptide Institute, Tokyo, Japan) for the indicated time intervals. After the harvested cells were lysed by TBS containing 0.1% SDS and 1% Nonidet P-40, immunoprecipitation was performed with anti-rhodopsin and FLAG antibodies.

Preparation of Recombinant Proteins and in Vitro Ubiquitylation Assay—The His-tagged Fbs1 ΔF, Fbs1 ΔP baculovirus were produced by Bac-to-Bac baculovirus expression system (Invitrogen). The SCF^{Fbs1}, Skp1-Fbs1 dimers, Fbs1 Fbs1 ΔF, Fbs1 ΔP, Skp1-ΔP dimers, and Fbs1 ΔN were obtained by baculovirus-infected HighFive cells as described previously (10). These proteins were purified by affinity chromatography using RNaseB-immobilized beads as a ligand and chitobiose as an eluent, and the eluates were dialyzed to 1,000 volumes of TBS three times. *In vitro* ubiquitylation assays were performed as described previously (10).

Aggregation Assay—Jack bean α-mannosidase (Sigma) was desalted using a NAP-25 gel filtration column (Amersham Biosciences) equilibrated in 10 mM Tris-HCl (pH 8.0). The desalted protein was lyophilized and redissolved at 21.7 μM in 0.1 M Tris-HCl (pH 8.0) and 6 M GdnHCl as described previously (13). After denaturation for 60 min at room temperature, samples were diluted to 0.3 μM in 1 ml of TBS containing various concentrations of bovine serum albumin or recombinant Fbs1 derivatives. Protein aggregation was monitored at 25 °C over a period of 60 min by measuring absorbance at 360 nm.

RESULTS

Multiple States of Fbs1 in Brain—Fbs1 has been found in the fraction eluted with di-*N*-acetyl-D-glucosamine (thereafter referred to as chitobiose) from GlcNAc-terminated fetuin of lysates prepared from mouse brain (8). Fbs1 and Skp1 proteins were detected in the eluted fraction with Coomassie Brilliant Blue staining, but we could not detect the apparent band of Cul1. However, the formation of the SCF^{Fbs1} complex was confirmed not only by reciprocal immunoprecipitation experiments in 293T cells but also by reconstitution of baculovirally expressed recombinant SCF^{Fbs1} proteins. To address these contradictory observations, we tested whether endogenous Fbs1 in the mouse brain forms the SCF complex by examining the interaction of Fbs1 with Cul1 (Fig. 1*A*). Fbs1 can be easily purified by affinity chromatography using RNaseB that contains a high mannose oligosaccharide as a ligand and chitobiose as an eluent (10). Since Fbs1 contains a single binding domain toward an *N*-glycan, it seems likely that the eluated Fbs1 protein or its complex from the RNaseB-immobilized resin is free from its substrates. Indeed, the glycoproteins modified with high mannose oligosaccharides were not included in the eluates by chitobiose (Fig. 1*B*). Although Skp1 was effectively co-immunoprecipitated with Fbs1 from the lysate of mouse brain, the amount of Skp1 that was eluted with Fbs1 from the RNaseB resin was small (Fig. 1*A*). Despite the difference in the quantities of Skp1 bound to Fbs1 in the fractions between eluates from

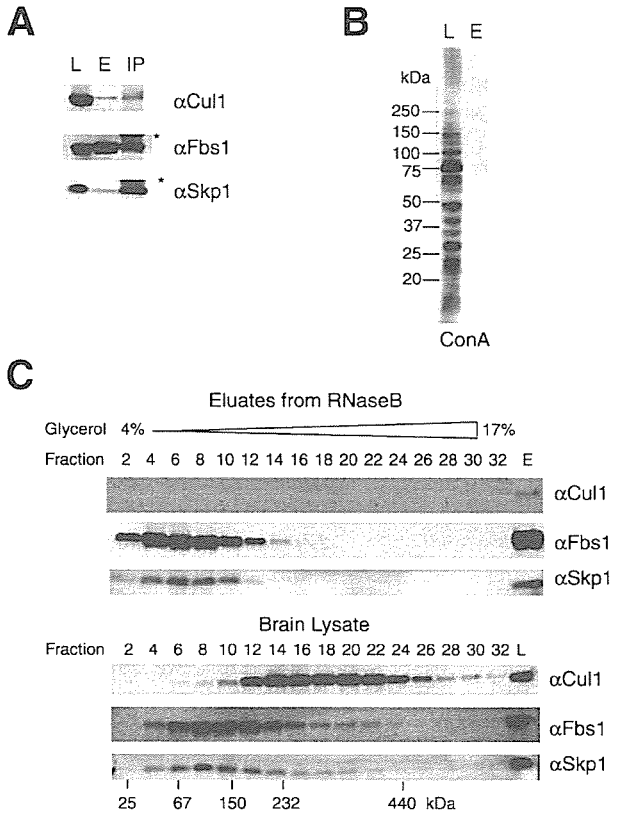

FIGURE 1. **States of Fbs1 in mouse brain.** *A*, 0.6 mg of lysate from adult mouse brain was subjected to RNaseB-immobilized affinity column and eluated with chitobiose (*E*) or subjected to immunoprecipitation with an antibody to Fbs1 (*IP*). Thirty μg of lysate (*L*), one-tenth of eluate, and immunoprecipitate were analyzed by immunoblotting with antibodies to Cul1, Fbs1, or Skp1. *Asterisks* show Ig heavy chain (*αFbs1*) and light chain (*αSkp1*). *B*, ConA lectin blot for brain lysate (*L*) and the eluate from the RNaseB resin (*E*) against the same amounts of proteins described in *A*. *C*, adult mouse brain lysate (*lower panel*, 0.7 mg) and lysate eluated with chitobiose from RNaseB (*upper panel*, started from 7 mg of the lysate) were separated by 4–17% glycerol density gradient centrifugation. One-third of each fraction was analyzed by immunoblotting with antibodies to Cul1, Fbs1, and Skp1. *Molecular size markers* are indicated below.

the RNaseB resin and immunoprecipitation with an anti-Fbs1 antibody, almost the same and small quantities of Cul1 were detected in these fractions. These results suggest that major populations of substrate-free Fbs1 and substrate-binding Fbs1 are present as Fbs1 monomers and Fbs1-Skp1 dimers, respectively, and the binding of substrates to Fbs1 does not influence the weak SCF complex formation.

To examine the behavior of endogenous Fbs1 in more detail, eluates from the RNaseB resin and lysates from the mouse brain were separated by a 4–17% glycerol density gradient centrifugation (Fig. 1*C*). The distribution of Fbs1 (~42 kDa) in the chitobiose eluates corresponded to the position of Fbs1 monomers (fraction 4) and Skp1-Fbs1 dimers (~63 kDa)(fraction 6). Although Cul1 was not detected in any fractions, the peak of Skp1 in eluates from the RNaseB resin was in the position of the Skp1-Fbs1 dimer. On the other hand, Fbs1 protein in brain lysate was detected in a broad range of fractions mainly larger than Fbs1-Skp1 dimers, indicating that most Fbs1, if not all, is associated with various glycoprotein substrates; *i.e.* Fbs1-Skp1 dimers maintain the association with glycoproteins *in vivo*. Cul1 (~90 kDa) in brain lysate was distributed broadly in higher density fractions, indicating its association with various other SCF-components.

Minor Population of Fbs1 Forms SCF Complex on ER—We next expressed FLAG-tagged F-box proteins alone or their combination with HA-tagged Skp1 in 293T cells and immunoprecipitated with anti-FLAG and anti-HA antibodies (Fig. 2*A*). The expression of HA-tagged Skp1 increased the amount of exogenous F-box proteins, suggesting that Skp1 stabilizes F-box proteins (*lanes 1–8*). Cul1 was co-immunoprecipitated with Fbs2 and Fbg3, which are highly homologous with Fbs1, or βTrCP1/Fbw1, one of the Fbw family members (*lanes 11–16*). The interaction between Cul1 and these F-box proteins increased upon co-expression of Skp1. However, unlike these F-box proteins, Fbs1 was almost undetectable in the immune complex with Cul1, regardless of the overexpression of exogenous Skp1 (*lanes 9* and *10*), although Fbs1 was co-immunoprecipitated with Skp1 as well as other F-box proteins (*lanes 18, 20, 22,* and *24* in the *αFlag panel*). Moreover, the amount of Cul1 associated with exogenous Skp1 was lower in the presence of Fbs1 than in those of other F-box proteins, suggesting that expression of Fbs1 prevents forming other SCF complexes by dimerizing with Skp1 (*lanes 18, 20, 22,* and *24* in the *αCul1 panel*). These results suggest that Fbs1 can strongly bind Skp1 but is weak in forming the SCF^{Fbs1} complex.

We have recently reported that Fbs1 is a cytosolic protein but that part of Fbs1 associates with the ER membrane through interaction with p97/VCP (valosin-containing protein) (11). We next examined whether the ER membrane-associated Fbs1 formed the SCF complex. Lysates of 293T and HeLa cells expressing FLAG-tagged Fbs1 were fractionated into the 100,000 × *g* supernatant and precipitate fractions excluding the 8,000 × *g* precipitate, and then Fbs1 was immunoprecipitated from these fractions by anti-FLAG antibody. As shown in Fig. 2*B*, Cul1 was co-immunoprecipitated with Fbs1 mainly from the precipitate (*p*) fraction (*lanes 4* and *8*). Although the association of Fbs1 with Skp1 occurred more effectively in the supernatant (*s*) fraction, the formation of the SCF complex, including Fbs1, was hardly detected in the supernatant fraction (*lanes 3* and *7*). Moreover, we examined whether endogenous Fbs1 formed the SCF complex in the precipitate fraction using nerve growth factor-treated PC12 cells, which endogenously express Fbs1 (14). As shown in Fig. 2*C*, part of Cul1 was co-immunoprecipitated with Fbs1 from the precipitate (*p*) fraction. These results indicate that the major population of endogenous Fbs1 is present as the Fbs1-Skp1 heterodimers or the Fbs1 monomers in the cytosol, and a minor population of Fbs1 forms the SCF complex bound on the ER membrane.

Linker Sequence of Fbs1 Prevents SCF Complex Formation—Although the SCF complex formation of Fbs1 was inefficient, Fbs2 formed the SCF complex effectively (Fig. 2*A*). To identify the region(s) of Fbs1 that impedes SCF complex formation, we examined the ability of various fusion proteins containing Fbs1 and Fbs2 fragments to form the complex and compared these findings with the full-length proteins in co-immunoprecipitation assay (Fig. 3*A*). Fbs1 ΔF was used as negative control that did not bind to Skp1 (Fig. 3*B*, *lane 3*). Fbs1 YW and Fbs1 ΔC, both of which are deficient in substrate binding, could not restore SCF complex formation, indicating that the interaction

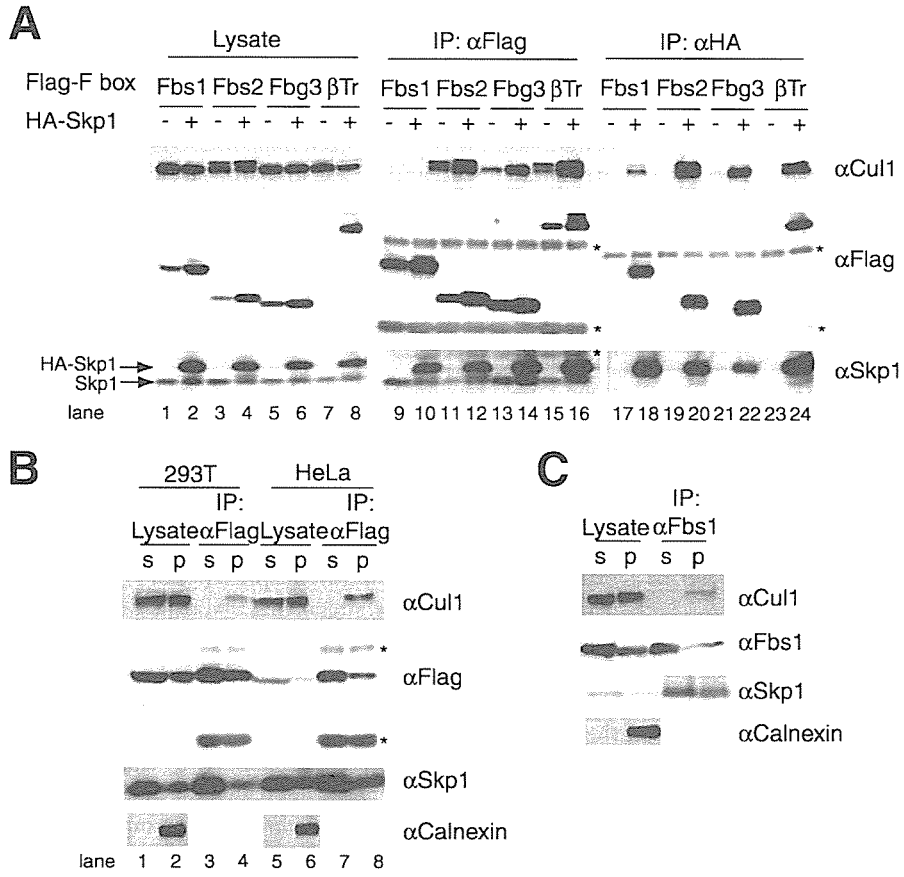

FIGURE 2. **Major population of Fbs1 forms non-SCF complex *in vivo*.** *A*, 293T cells were transfected with plasmids encoding various FLAG-tagged F-box proteins (Fbs1, Fbs2, Fbg3, and βTrCP1 (*βTr*)) combination with empty HA plasmids (−) or plasmids encoding HA-tagged Skp1 (+). Whole cell lysates were subjected to immunoprecipitation (*IP*) with antibodies to FLAG and HA, and lysates (15 μg each) and one half of the resulting precipitates were analyzed by immunoblotting with antibodies to Cul1, FLAG, and Skp1. *Asterisks* show Ig heavy and light chains. *B*, 293T and HeLa cells were transfected with FLAG-tagged Fbs1. Cell lysates were fractionated by ultracentrifugation, and FLAG-Fbs1 was immunoprecipitated with an antibody to FLAG from the same amount of proteins of 100,000 × *g* supernatant (*s*) and precipitate (*p*) fractions. The total amount of protein of the supernatant fraction was 2–3 times larger than that of the precipitate fraction. Lysates (15 μg each) and immunoprecipitates were analyzed by immunoblotting with antibodies to Cul1, FLAG, and Skp1. *Asterisks* show Ig heavy and light chains. To control for the fractionation, immunoblotting with an antibody to calnexin was performed. *C*, endogenous Fbs1 was immunoprecipitated with an antibody to Fbs1 from 100,000 × *g* supernatant, and precipitate fractions of differentiated PC12 cells were treated with nerve growth factor. Lysates (15 μg each) and immunoprecipitates were analyzed by immunoblotting. The immunoblotting analysis for separated supernatant and precipitate fractions was conducted as for *B*.

between Fbs1 and its substrates does not affect the complex formation (*lanes 4* and *5*). The N-terminal sequence of Fbs1 called the P domain is unique and is not seen in other F-box proteins, but the removal of this domain from Fbs1 or the addition to Fbs2 did not affect the complex formation (Fbs1 ΔP and Fbs2 P1: *lanes 6* and *13*). Exchange of the F-box domains between Fbs1 and Fbs2 caused the loss of the Skp1 binding activity, probably due to the incorrect folding (Fbs1 F2, Fbs1 ΔPF2, Fbs2 F1, and Fbs2 PF1: *lanes 7*, *8*, *10*, and *11*, respectively). However, the replacement of the Fbs1 N-terminal region (which contains P and F-box domains and linker sequence) with the Fbs2 N-terminal region rescued the complex formation (Fbs-2N1C: *lane 9*). In contrast, the addition of the Fbs1 N-terminal region instead of the Fbs2 N-terminal region markedly reduced the activity of Fbs2 to form the SCF complex but did not affect the Skp1 binding (Fbs-1N2C: *lane 12*). The linker sequences of the intervening segments between the F-box domain and the substrate-binding domain showed lower homology than other portions between Fbs1 and Fbs2, suggesting that the Fbs1 linker sequence is responsible for impeding the SCF^{Fbs1} complex formation. Indeed, only the Fbs1 mutant protein that contained the Fbs2 linker sequence could form the SCF complex, but the efficiency of the SCF complex formation was less than that of Fbs-2N1C (Fbs1 I2: *lane 15*). On the other hand, Fbs2 protein containing the Fbs1 linker sequence and the Fbs1 protein without its linker sequence did not seem to show the correct folding for Skp1 binding (Fbs2 I1 and Fbs1 ΔI: *lanes 16* and *17*). The Fbs1 mutant in which the F-box domain and the linker sequence are replaced with those of Fbs2 forms the SCF complex effectively. Thus, we conclude that the Fbs1 linker sequence between the F-box and substrate-binding domains hampers the SCF^{Fbs1} complex formation.

We next compared the localization of Fbs1, Fbs2, and the mutant Fbs1 proteins capable of forming the SCF complex: Fbs-2N1C and Fbs1 I2 (Fig. 3*C*). Although a minor population of Fbs1 in the precipitate (*p*) fraction formed the SCF complex, most Fbs2 formed the SCF^{Fbs2} complex in the supernatant (*s*) fraction as well as the precipitate fraction. Fbs-2N1C could form the SCF complex mainly in the supernatant fraction (Fig. 3*C*). Moreover, the amount of Cul1 co-immunoprecipitated with Fbs1 I2 was similar in both fractions. These results suggest that the linker sequence of Fbs1 does not only impede the formation of the SCF complex but also restricts the localization of the SCF complex bound on the ER membrane.

Expression of Mutant Fbs1 That Forms E3 Easily Induces Proteolysis of Its Substrates—To confirm that most Fbs1 in the cells is inactive to function as an E3 ubiquitin ligase, we next examined the ability of the mutant Fbs1 that readily forms the SCF complex (Fbs-2N1C) to ubiquitylate the substrates. It has been shown that P23H mutated rhodopsin (hereafter referred to as P23H) is an ERAD substrate, and its *N*-linked glycosylation is required for the degradation (15, 16). As reported previously, rhodopsin monomer is ~40–43 kDa, but the majority of P23H was detected as high molecular weight complex multimers by immunoblotting with anti-rhodopsin antibody (Fig. 4*A*). Wild-type Fbs1, but not the substrate-binding defective mutant Fbs1 YW, was able to associate with P23H effectively, suggesting that Fbs1 binds to P23H through its *N*-glycans. On the other hand,

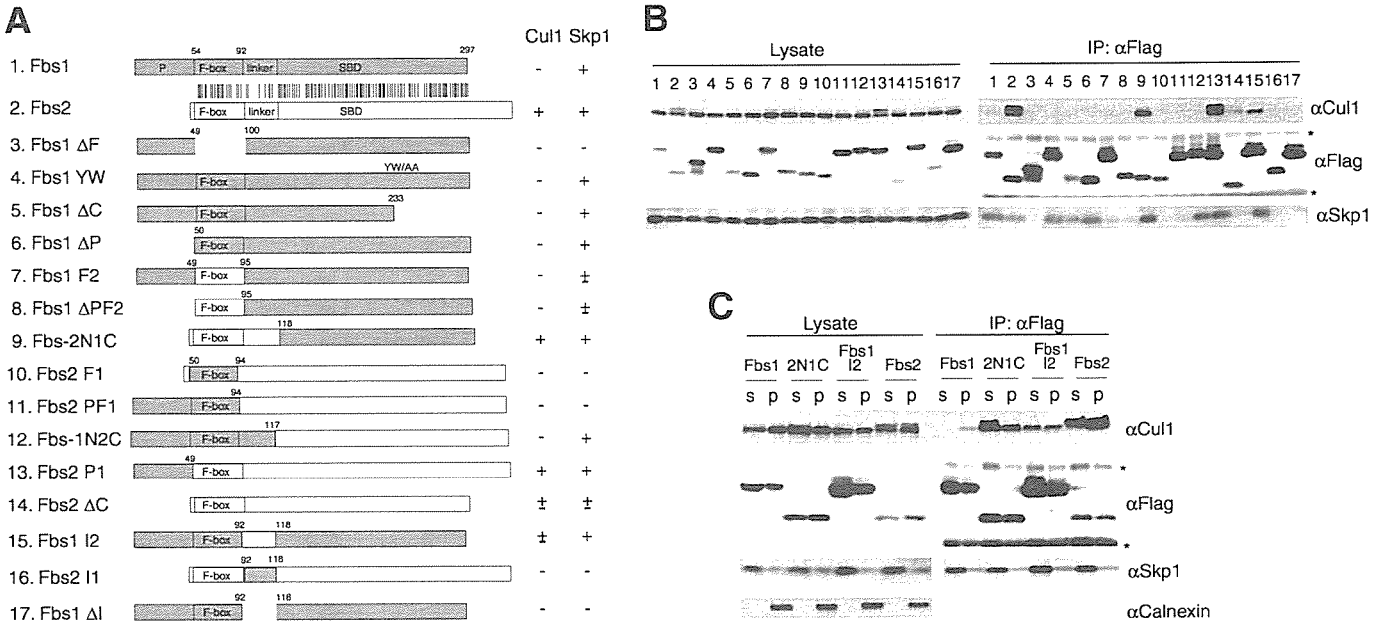

FIGURE 3. **Linker sequence between F-box and substrate-binding domains of Fbs1 hampers SCF^{Fbs1} complex formation.** *A*, schematic representation of constructs of fusion proteins consisting of Fbs1 and Fbs2 fragments. The fragments derived from Fbs1 and Fbs2 appear in *gray* and *white boxes*, respectively. The *numbers* above the constructs represent the amino acid position of Fbs1. The *vertical bars* represent identical amino acids between Fbs1 and Fbs2. P and F-box domains, linker sequence, and sugar-binding domain are represented by *P*, *F-box*, *linker*, and *SBD*, respectively. The binding activities of these constructs toward Cul1 and Skp1 shown in *B* are summarized on the *right*, with + representing strong binding, + representing weak binding, and − representing no binding. *B*, 293T cells were transfected with plasmids encoding the FLAG-tagged mutants F-box proteins represented in *A*. Whole cell lysates were subjected to immunoprecipitation (*IP*) with an antibody to FLAG, and the resulting precipitates were analyzed by immunoblotting with antibodies to Cul1, Skp1, and FLAG. *Asterisks* show Ig heavy and light chains. *C*, 293T cells were transfected with FLAG-tagged Fbs1, Fbs-2N1C, Fbs1 I2, or Fbs2. Cell lysates were fractionated by ultracentrifugation, and FLAG-Fbs1 was immunoprecipitated with an antibody to FLAG from 100,000 × *g* supernatant (*s*) and precipitate (*p*) fractions. The resulting immunoprecipitates were analyzed by immunoblotting as in Fig. 2*B*.

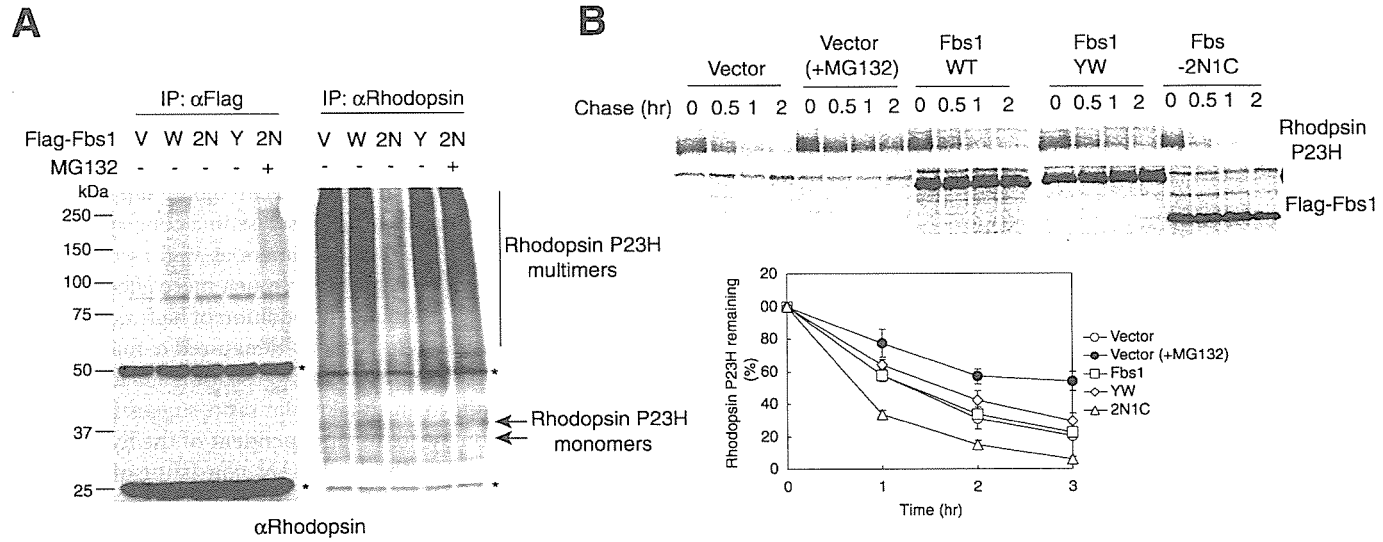

FIGURE 4. **Expression of Fbs-2N1C promotes substrate degradation.** *A*, 293T cells were transfected with plasmids encoding FLAG-tagged empty vector (*V*), Fbs1 (*W*), Fbs-2N1C (*2N*), or Fbs1 YW (*Y*) and combination with rhodopsin P23H mutant. Some cells were treated with 10 μM MG132 for 16 h. Whole cell lysates were subjected to immunoprecipitation (*IP*) with antibodies to FLAG and rhodopsin, and the resulting precipitates were analyzed by immunoblotting with an antibody to rhodopsin. *Asterisks* show Ig heavy and light chains. *B*, rhodopsin P23H was co-transfected with FLAG-tagged empty vector, Fbs1, Fbs-2N1C, or Fbs1 YW. Twenty-four hours after transfection, 293T cells were pulse-labeled with [^{35}S]Met/Cys for 1 h and chased for the indicated time intervals. Rhodopsin P23H and Fbs1 derivatives were immunoprecipitated with antibodies to rhodopsin and FLAG, respectively. The plotted data at the bottom show a quantification analysis of the stability of rhodopsin P23H over time in the *upper panels*. Data are the mean ± S.D. of three independent experiments. *WT*, wild type.

Fbs-2N1C could bind to P23H, although its binding to P23H seemed weaker than that of wild-type Fbs1 (Fig. 4*A*, *left panel*). Since the activity to bind RNaseB was not different between Fbs1 and Fbs-2N1C (data not shown), it seems likely that the $SCF^{Fbs\text{-}2N1C}$ causes degradation of P23H through its ubiquitylation. Interestingly, the quantity of P23H decreased upon Fbs-2N1C expression (Fig. 4*A*, *right panel*). It has been reported that the degradation of P23H was suppressed by MG132 treatment (15, 16). The quantities of both P23H associated with Fbs-2N1C and the P23H protein were recovered by the addition of MG132. Moreover, we performed pulse-chase analysis using 293T cells co-expressing the P23H mutant and FLAG-tagged

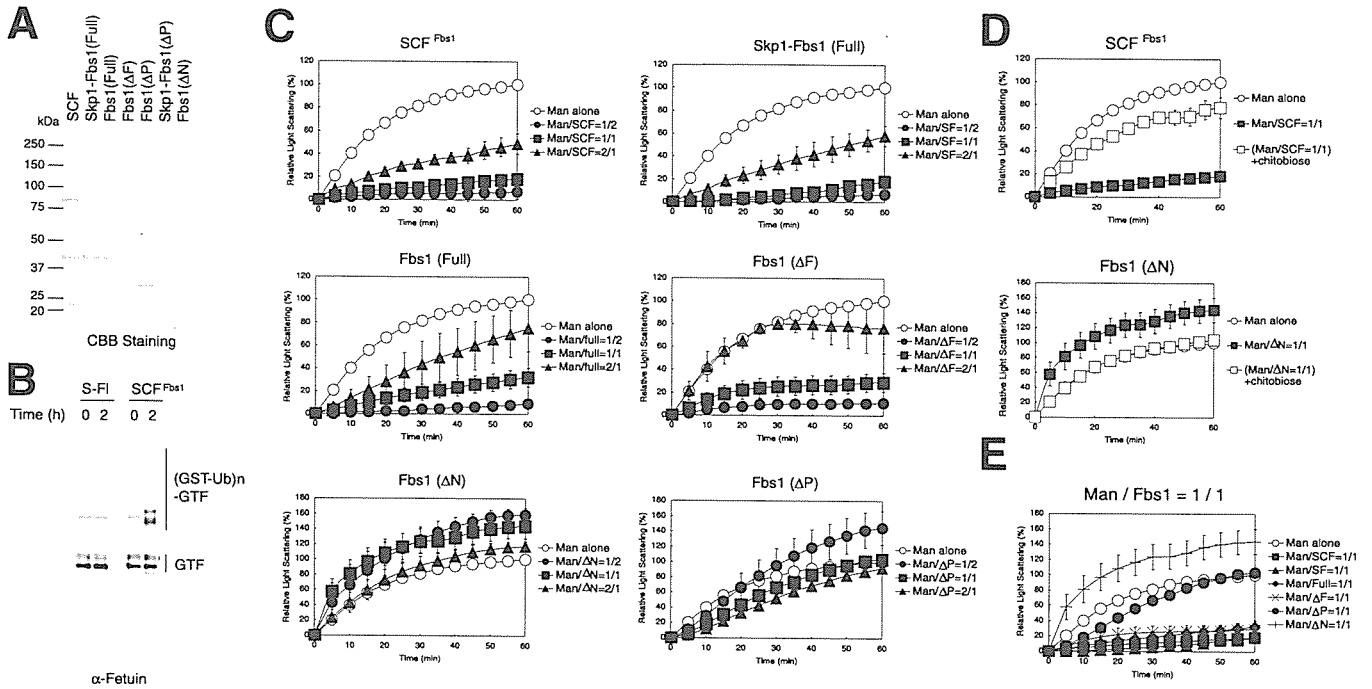

FIGURE 5. **Fbs1 complexes suppress the aggregation of denatured α-mannosidase *in vitro*.** *A*, electrophoretic pattern of the recombinant proteins produced by the baculovirus system. *CBB Staining*, Coomassie Brilliant Blue staining. *B*, GlcNAc-terminated fetuin (*GTF*) was incubated in a reaction mixture containing the ATP-regenerating system, recombinant ubiquitin-activating enzyme (E1), Ubc4, GST-ubiquitin (*GST-Ub*), and Skp1-Fbs1 dimer (*S-Fl*) or SCF complex (*SCF*) in the presence of the NEDD8 system at 30 °C. The high molecular mass ubiquitylated fetuin ((*GST-Ub*)*n-GTF*) was detected by immunoblotting with anti-fetuin antibody. *C*, after denaturation in 6 M GdnHCl, α-mannosidase (*Man*) was diluted to a final concentration of 0.3 mM at 25 °C in the presence of the indicated concentrations of SCF^{Fbs1} (*SCF^{Fbs1}* or *SCF*), Skp1 and Fbs1 dimer (*Skp1-Fbs1 (Full)* or *SF*), Fbs1 monomer (*Fbs1 (Full)* or *Full*), or Fbs1 derivatives (*ΔF*, *ΔN*, or *ΔP*). Aggregation was measured by monitoring light scattering at 360 nm over a period of 60 min. Data are the mean ± S.D. of at least three independent experiments. *D*, α-mannosidase was allowed to aggregate in the presence of equal mole of SCF^{Fbs1} or Fbs1 (ΔN). 0.05 mM *N*, *N*′-diacetylchitobiose was added (+chitobiose), and the effects on aggregation were monitored by measuring light scattering at 360 nm. Data are the mean and standard deviation of three independent experiments. *E*, α-mannosidase was allowed to aggregate in the presence of equal mole of recombinant Fbs1 complexes or derivatives. Data are the mean ± S.D. of three independent experiments.

Fbs1 derivatives. The degradation of P23H was suppressed by MG132 treatment as reported previously (Fig. 4*B*). Although wild-type Fbs1 or the YW mutant did not influence the kinetics of P23H degradation, co-expression of Fbs-2N1C efficiently promoted its degradation. On the other hand, like wild-type Fbs1, Fbs1 I2, could associate with P23H, but its expression did not influence both the amount of P23H and the kinetics of P23H degradation (data not shown). These results demonstrate that the non-SCF complex of Fbs1 can be converted to an active E3 ligase by introducing the complex-forming activity mapped onto the F-box domain and the linker sequence of Fbs2.

Fbs1 Suppresses Aggregation of Denatured Glycoprotein in Vitro—We reported previously that the expression of Fbs1 inhibits aggresome formation in Cos7 cells (8). Furthermore, since Fbs1 interacts with denatured glycoproteins more efficiently than native glycoproteins, we examined whether Fbs1 functions as a molecular chaperone for glycoproteins *in vitro*. To this end, we prepared recombinant SCF^{Fbs1}, Skp1-Fbs1 dimers, Fbs1, Fbs1 ΔF, Fbs1 ΔP, Skp1-ΔP dimers, and Fbs1 ΔN, all of which were produced by using a baculovirus system (Fig. 5*A*). To obtain highly purified recombinant proteins, we purified them by using the affinity for the RNaseB resin but not nickel resin toward His tag. The purified SCF^{Fbs1} but not Skp1-Fbs1 dimers could ubiquitylate GlcNAc-terminated fetuin (*GTF*) effectively (Fig. 5*B*). We next assessed the ability of these proteins or their complexes to suppress the aggregation by using denatured α-mannosidase that contains high mannose type oligosaccharides, a typical substrate for the glycoprotein aggregation assay (17). Although Fbs1 alone suppressed the aggregation of denatured α-mannosidase in a concentration-dependent manner, the Fbs1-Skp1 dimers as well as the SCF^{Fbs1} complex suppressed the aggregation much more effectively than Fbs1 alone (Fig. 5*C*). Although the addition of half-molar of Fbs1 ΔF did not affect the aggregation of denatured α-mannosidase, ΔF was also active to suppress the aggregation at a level similar to that of Fbs1 alone in an equal molar ratio, suggesting that the partial suppression by Fbs1 is independent of the hydrophobic F-box domain. On the other hand, ΔN, consisting of substrate-binding domain alone, enhanced its aggregation. Both the aggregation-suppressing activity of SCF^{Fbs1}, Skp1-Fbs1 dimers, or Fbs1 and the aggregation-enhancing activity of ΔN were inhibited by chitobiose (Fig. 5*D* and not shown). In contrast, these recombinant Fbs1 protein complexes had no effect on the aggregation of non-glycosylated proteins such as citrate synthase and luciferase (data not shown). Importantly, ΔP as well as the Skp1-ΔP dimers could not suppress the aggregation of α-mannosidase in an equal molar ratio (Fig. 5, *C* and *E*, and not shown). These results indicate that the Skp1-Fbs1 dimers effectively suppress the aggregation of denatured glycoproteins by recognizing the exposed chitobiose in *N*-glycans and that the P domain of Fbs1 is required for this aggregation suppressing activity.

DISCUSSION

The F-box family of proteins, which are the substrate-recognition subunits of the SCF ubiquitin ligase, play important roles in ubiquitin-dependent proteolysis in eukaryotes (18, 19). However, it is not clear whether all F-box proteins indeed function as receptor subunits of SCF complexes. For example, it has been reported that at least two F-box proteins, Ctfl3 and Rcy1, out of 11 F-box proteins in *Saccharomyces cerevisiae*, do not form SCF complexes (20–22). Since not all RING-finger proteins are ubiquitin ligases, it is possible that non-canonical F-box proteins that fail to form the SCF complex play some important roles other than ubiquitin ligase activity. In the present study, we showed that the SCF complex formation of Fbs1, which recognizes *N*-glycans, is not efficient and that the intervening segment between the F-box domain and the sugar-binding domain of Fbs1 suppresses the formation of the SCF complex. The major population of Fbs1 is present as Fbs1-Skp1 heterodimers or Fbs1 monomers, which can inhibit the aggregation of the glycoproteins. Our results show that Fbs1 contributes to a chaperone function in addition to the role of the SCF^{Fbs1} ubiquitin ligase, opening new perspectives for cellular activities of F-box proteins.

Although most endogenous Fbs1 was not assembled into the SCF^{Fbs1} complex, a minor population of Fbs1 was capable of forming the SCF^{Fbs1} complex in cells. Moreover, the SCF^{Fbs1} complex could be produced in insect cells by infection with the baculovirus, indicating that Fbs1 can intrinsically form the SCF complex. It is worth noting that the SCF^{Fbs1} was mainly present in the 100,000 × *g* precipitate fraction including the microsome (Fig. 2, *B* and *C*). It is not clear why the SCF^{Fbs1} is bound to the ER membrane, although it is plausible that it plays a pivotal role in the ERAD pathway. To examine how the SCF complex formation of Fbs1 was promoted *in vivo*, we treated Fbs1-expressing cells with ER stress inducers, such as thapsigargin and dithiothreitol or a proteasome inhibitor MG132. These treatments, however, did not affect the SCF complex formation (data not shown). Furthermore, although the interaction between Fbs1 and its substrate glycoproteins did not affect the SCF complex formation (Figs. 1*A* and 3*B*), we examined the effects of overexpression of p97/VCP, Fbs1 substrates, Skp1, or Cul1. No protein other than Cul1 accelerated the SCF^{Fbs1} formation not only in the 100,000 × *g* precipitate fraction but also in the cytosol (Fig. 2*A* and data not shown). Intriguingly, whereas Fbs1 and Skp1 were mainly located in the cytosol (100,000 × *g* supernatant fraction), Cul1 was detected not only in the cytosol but also in the 100,000 × *g* precipitate fraction (Figs. 2, *B* and *C*, and 3*C*), suggesting that Cul1 is recruited to the microsome membrane where the SCF^{Fbs1} complex will be assembled to ubiquitylate efficiently the *N*-linked glycosylated ERAD substrates.

Fbs1 belongs to a subfamily consisting of at least five homologous F-box proteins that contain a conserved FBA motif in their C termini (5, 6). Among them, at least Fbs2 recognizes high mannose oligosaccharides as well as Fbs1 and forms an SCF-type ubiquitin ligase. The Fbs1 protein sequence shows highly homologous to that of Fbs2 other than the P domain of Fbs1 and C-terminal part of Fbs2, but the linker sequence between the F-box and FBA domains shows lower homology than other portions (Fig. 3*A*). As shown in Fig. 3*B*, the difference in the ability for assembling into the SCF complex between Fbs1 and Fbs2 is ascribed to the short linker sequence (92–117 amino acids of Fbs1). Although Fbs2 formed the SCF complex efficiently in the cytosol as well as the 100,000 × *g* precipitate fraction, the SCF^{Fbs1} formation was mainly present bound on the ER membrane (Fig. 3*C*). Although it is not clear whether the linker sequence of Fbs1 prevents the SCF^{Fbs1} from being in the cytosol or causes the formation of the SCF^{Fbs1} bound on the ER membrane, this limited localization of SCF^{Fbs1} is also due to the linker sequence (Fig. 3*C*). Crystal structure and mutational analyses of Cdc4 and βTrCP1 revealed the importance of orientation and rigidity in the linker sequence between F-box and WD40 domains for their *in vivo* function (23, 24). The linker sequences of Cdc4 and βTrCP1 are longer than that of Fbs1 and form three or four helix globular domains. On the other hand, the linker sequence of Fbs1 is an unstructured domain that consists of a flexible linker loop and an α-helix and is too far from Cul1 to influence directly the SCF complex formation.[3] The information of the structure of Skp1-Fbs1 suggests that the prevention of the SCF complex formation by this unstructured linker sequence can be cancelled by binding to the membrane or unidentified proteins on the ER.

In this study, we demonstrated that the Fbs1 could suppress the aggregation of denatured glycoproteins. This activity is due to the N-terminal P domain that is not seen in other F-box proteins. This N-terminal domain has been reported as a PEST sequence rich in proline, glutamic acid, serine, and threonine, which are often found in short-lived proteins (25). The N-terminal sequence in Fbs1, however, did not seem to act as a general PEST because the deletion of the P domain from Fbs1 or the addition to Fbs2 did not affect the protein stability (Fig. 3). More recently, it has been reported that U-box type E3 CHIP (C terminus of Hsc-70-interacting protein) is associated with Fbs1 through the P domain (26). Although we did not detect the E3 activity of the Skp1-Fbs1 dimers produced in the insect cells toward glycoprotein substrate GlcNAc-terminated fetuin (Fig. 5*B*), it is possible that an unknown chaperone molecule of insect cells was bound to the P domain of Fbs1. Skp1-Fbs1 dimers and Fbs1 monomers as well as the SCF^{Fbs1} complex showed activity to suppress the denatured glycoprotein aggregation, suggesting that the majority of Fbs1 is present as Skp1-Fbs1 dimers or Fbs1 monomers in cells and is not an intermediate prior to assembly of the SCF^{Fbs1} complex, but rather, a novel functional unit.

It is predicted that more than 30% of eukaryotic proteins contain substantial regions of disordered structure (27). One feature of intrinsically disordered proteins is their rapid degradation. Intracellular protein quality control, especially the degradation of proteins with aberrant structures, is thought to be important particularly in quiescent cells such as neurons (28). Fbs1 is expressed mainly in neuronal cells in the adult brain (14). Recently, it has been reported (29, 30) that loss of autophagy leads to neurodegeneration even in the absence of any

[3] Mizushima, T., Yoshida, Y., Kumanomidou, T., Hasegawa, Y., Suzuki, A., Yamane, T., and Tanaka, K., unpublished data.

aggregation-prone mutant proteins. Moreover, these reports have shown that the primary role of autophagy under normal conditions is the turnover of diffused cytosolic proteins, rather than direct elimination of inclusion bodies (29, 30). Our study suggests that Fbs1 contributes to the clearance of such cytosolic proteins by constitutive autophagy, like other chaperone systems, to suppress the aggregation of abnormal glycoproteins in neurons. For this, the N-terminal unique sequence of Fbs1, the P domain, having chaperone function, may have been made up during evolution. Since Cul1 is a common component of the SCF complexes and Fbs1 is abundant in neuronal cells, Fbs1 may also evolutionally acquire the linker sequence that suppresses the SCF^{Fbs1} complex formation to supply Cul1 toward other F-box proteins. It also seems possible that Fbs1 functions as a chaperone to keep the solubility of a particular glycoprotein(s) in the cytosol in neuronal cells. Further studies are needed to identify the Fbs1 target glycoproteins in neuronal cells, which may reveal the role of Fbs1 in maintaining homeostasis of neuronal cells.

Acknowledgment—We thank M. E. Cheetham for generously providing rhodopsin constructs.

REFERENCES

1. Feldman, R. M., Correll, C. C., Kaplan, K. B., and Deshaies, R. J. (1997) *Cell* **91,** 221–230
2. Skowyra, D., Craig, K. L., Tyers, M., Elledge, S. J., and Harper, J. W. (1997) *Cell* **91,** 209–219
3. Bai, C., Sen, P., Hofmann, K., Ma, L., Goebl, M., Harper, J. W., and Elledge, S. J. (1996) *Cell* **86,** 263–274
4. Jin, J., Cardozo, T., Lovering, R. C., Elledge, S. J., Pagano, M., and Harper, J. W. (2004) *Genes Dev.* **18,** 2573–2580
5. Ilyin, G. P., Serandour, A. L., Pigeon, C., Rialland, M., Glaise, D., and Guguen-Guillouzo, C. (2002) *Gene (Amst.)* **296,** 11–20
6. Winston, J. T., Koepp, D. M., Zhu, C., Elledge, S. J., and Harper, J. W. (1999) *Curr. Biol.* **9,** 1180–1182
7. Yoshida, Y., Tokunaga, F., Chiba, T., Iwai, K., Tanaka, K., and Tai, T. (2003) *J. Biol. Chem.* **278,** 43877–43884
8. Yoshida, Y., Chiba, T., Tokunaga, F., Kawasaki, H., Iwai, K., Suzuki, T., Ito, Y., Matsuoka, K., Yoshida, M., Tanaka, K., and Tai, T. (2002) *Nature* **418,** 438–442
9. Mizushima, T., Hirao, T., Yoshida, Y., Lee, S. J., Chiba, T., Iwai, K., Yamaguchi, Y., Kato, K., Tsukihara, T., and Tanaka, K. (2004) *Nat. Struct. Mol. Biol.* **11,** 365–370
10. Yoshida, Y. (2005) *Methods Enzymol.* **398,** 159–169
11. Yoshida, Y., Adachi, E., Fukiya, K., Iwai, K., and Tanaka, K. (2005) *EMBO Rep.* **6,** 239–244
12. Tanahashi, N., Murakami, Y., Minami, Y., Shimbara, N., Hendil, K. B., and Tanaka, K. (2000) *J. Biol. Chem.* **275,** 14336–14345
13. Paquet, M. E., Leach, M. R., and Williams, D. B. (2005) *Methods (Oxf.)* **35,** 338–347
14. Erhardt, J. A., Hynicka, W., DiBenedetto, A., Shen, N., Stone, N., Paulson, H., and Pittman, R. N. (1998) *J. Biol. Chem.* **273,** 35222–35227
15. Illing, M. E., Rajan, R. S., Bence, N. F., and Kopito, R. R. (2002) *J. Biol. Chem.* **277,** 34150–34160
16. Saliba, R. S., Munro, P. M., Luthert, P. J., and Cheetham, M. E. (2002) *J. Cell Sci.* **115,** 2907–2918
17. Stronge, V. S., Saito, Y., Ihara, Y., and Williams, D. B. (2001) *J. Biol. Chem.* **276,** 39779–39787
18. Cardozo, T., and Pagano, M. (2004) *Nat Rev. Mol. Cell. Biol.* **5,** 739–751
19. Petroski, M. D., and Deshaies, R. J. (2005) *Nat. Rev. Mol. Cell. Biol.* **6,** 9–20
20. Galan, J. M., Wiederkehr, A., Seol, J. H., Haguenauer-Tsapis, R., Deshaies, R. J., Riezman, H., and Peter, M. (2001) *Mol. Cell. Biol.* **21,** 3105–3117
21. Kaplan, K. B., Hyman, A. A., and Sorger, P. K. (1997) *Cell* **91,** 491–500
22. Russell, I. D., Grancell, A. S., and Sorger, P. K. (1999) *J. Cell Biol.* **145,** 933–950
23. Orlicky, S., Tang, X., Willems, A., Tyers, M., and Sicheri, F. (2003) *Cell* **112,** 243–256
24. Wu, G., Xu, G., Schulman, B. A., Jeffrey, P. D., Harper, J. W., and Pavletich, N. P. (2003) *Mol. Cell* **11,** 1445–1456
25. Rechsteiner, M., and Rogers, S. W. (1996) *Trends Biochem. Sci.* **21,** 267–271
26. Nelson, R. F., Glenn, K. A., Miller, V. M., Wen, H., and Paulson, H. L. (2006) *J. Biol. Chem.* **281,** 20242–20251
27. Fink, A. L. (2005) *Curr. Opin. Struct. Biol.* **15,** 35–41
28. Forman, M. S., Trojanowski, J. Q., and Lee, V. M. (2004) *Nat. Med.* **10,** 1055–1063
29. Hara, T., Nakamura, K., Matsui, M., Yamamoto, A., Nakahara, Y., Suzuki-Migishima, R., Yokoyama, M., Mishima, K., Saito, I., Okano, H., and Mizushima, N. (2006) *Nature* **441,** 885–889
30. Komatsu, M., Waguri, S., Chiba, T., Murata, S., Iwata, J., Tanida, I., Ueno, T., Koike, M., Uchiyama, Y., Kominami, E., and Tanaka, K. (2006) *Nature* **441,** 880–888

Structural basis for the selection of glycosylated substrates by SCF^{Fbs1} ubiquitin ligase

Tsunehiro Mizushima*†, Yukiko Yoshida‡, Taichi Kumanomidou*, Yuko Hasegawa*, Atsuo Suzuki*, Takashi Yamane*§, and Keiji Tanaka‡§

*Department of Biotechnology, Graduate School of Engineering, Nagoya University, Chikusa-ku, Nagoya 464-8603, Japan; †Precursory Research for Embryonic Science and Technology, Japan Science and Technology Agency, Kawaguchi, Saitama 332-0012, Japan; and ‡Laboratory of Frontier Science, Tokyo Metropolitan Institute of Medical Science, Bunkyo-ku, Tokyo 113-8613, Japan

Edited by John Kuriyan, University of California, Berkeley, CA, and approved February 21, 2007 (received for review November 21, 2006)

The ubiquitin ligase complex SCF^{Fbs1}, which contributes to the ubiquitination of glycoproteins, is involved in the endoplasmic reticulum-associated degradation pathway. In SCF ubiquitin ligases, a diverse array of F-box proteins confers substrate specificity. Fbs1/Fbx2, a member of the F-box protein family, recognizes high-mannose oligosaccharides. To elucidate the structural basis of SCF^{Fbs1} function, we determined the crystal structures of the Skp1–Fbs1 complex and the sugar-binding domain (SBD) of the Fbs1–glycoprotein complex. The mechanistic model indicated by the structures appears to be well conserved among the SCF ubiquitin ligases. The structure of the SBD–glycoprotein complex indicates that the SBD primarily recognizes $Man_3GlcNAc_2$, thereby explaining the broad activity of the enzyme against various glycoproteins. Comparison of two crystal structures of the Skp1–Fbs1 complex revealed the relative motion of a linker segment between the F-box and the SBD domains, which might underlie the ability of the complex to recognize different acceptor lysine residues for ubiquitination.

glycoprotein | tertiary structure | ubiquitin system

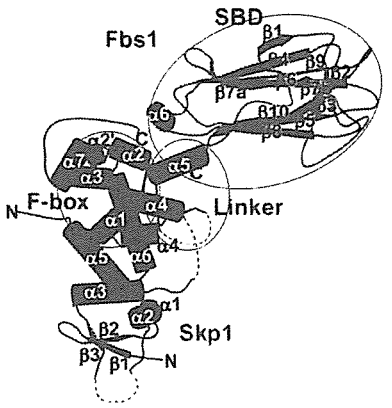

Fig. 1. Structure of the Skp1–Fbs1 complex. Skp1 and Fbs1 are colored blue and red, respectively. The secondary structure elements for Skp1 and Fbs1 are labeled. Dotted lines represent disordered regions. The F-box, linker, and SBD domains of Fbs1 are circled.

Ubiquitin-mediated proteolysis plays a regulatory role in a number of diverse cellular processes and involves the selective destruction of short-lived functional proteins (1). The ubiquitin–proteasome system also is responsible for the disposal of misfolded and unfolded cellular proteins, the aberrant accumulation of which usually causes cell death, which can lead to neurodegenerative diseases (2). Protein ubiquitination is catalyzed by a sophisticated cascade system consisting of the ubiquitin-activating (E1), ubiquitin-conjugating (E2), and ubiquitin-ligating (E3) enzymes (3). Among these enzymes, the E3 enzymes are responsible for the selection of target proteins. E3 enzymes are a diverse family of proteins and protein complexes. One of the best characterized groups of E3 enzymes is the SCF complex [composed of Skp1, Cul1, Rbx1 (also called Roc1), and an F-box protein], which regulates the degradation of a broad range of cellular proteins (4). F-box proteins consist of an N-terminal ≈40-aa F-box domain that binds to Skp1 and various C-terminal substrate-recognition regions and are subcategorized into three classes according to their substrate-binding domains. The Fbw (or FBXW) and Fbl (or FBXL) families possess WD40 repeats and leucine-rich repeats in their binding domains, respectively (5). The third class of F-box proteins is the Fbx (or FBXO) family, which does not contain any presumptive functional domains. However, we recently identified a subfamily within the Fbx family that consists of at least five homologous F-box proteins that recognize N-glycan; we named the sugar-binding domain (SBD)-containing proteins of this subfamily the Fbs (F-box protein that recognizes sugar chains; known previously as FBG) proteins (6).

In the SCF complex, Cul1 functions as a molecular scaffold that simultaneously interacts through its N and C termini with the crucial adaptor subunits Skp1 and Rbx1 together with a specific E2 enzyme, respectively. Skp1 is an adaptor protein that links Cul1 and one of the F-box proteins (6). Fbw and Fbl proteins usually recognize the phosphorylation status of the substrate, and structural models of the SCF complexes of some of these proteins, such as Fbw1/β-TrCP1 (7), Fbw7/Cdc4 (8), and Fbl1/Skp2 (9–11), have been reported. Structural information, however, is available only for the recognition of phosphorylated protein substrates.

N-linked glycosylation of proteins takes place in the endoplasmic reticulum and plays a key role in protein quality control (12). Misfolded proteins and unassembled protein complexes that fail to assume their functional states in the endoplasmic reticulum are subjected to endoplasmic reticulum-associated degradation, which involves retrotranslocation into the cytosol and degradation by the ubiquitin–proteasome system. SCF^{Fbs1} is an N-linked glycoprotein-specific ubiquitin ligase complex that contains the neuron-specific F-box protein Fbs1/Fbx2/NFB42 (13–16). We previously reported x-ray crystal structures of the Fbs1 SBD alone and in complex with di-*N*-acetylchitobiose (chitobiose, GlcNAc-GlcNAc, or $GlcNAc_2$), which revealed that the binding site is formed by a small hydrophobic pocket located at the top of a β-sandwich (17). The molecular mechanism

Author contributions: T.Y. and K.T. designed research; T.M., Y.Y., T.K., and Y.H. performed research; A.S. analyzed data; and T.M., Y.Y., and K.T. wrote the paper.

The authors declare no conflict of interest.

This article is a PNAS Direct Submission.

Abbreviations: RNaseB, ribonuclease B; SBD, sugar-binding domain.

Data deposition: The atomic coordinates and structure factors have been deposited in the Protein Data Bank, www.pdb.org (PDB ID codes 2E31, 2E32, and 2E33).

§To whom correspondence may be addressed. E-mail: yamane@nubio.nagoya-u.ac.jp or tanakak@rinshoken.or.jp.

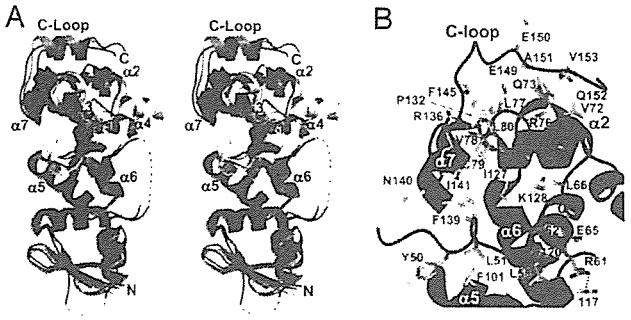

Fig. 2. Structure of the Skp1–Fbs1 interface. (*A*) Stereo views of the Fbs1 F-box domain (red) and Skp1 (blue) are compared with the structures of Skp1–Skp2 and Skp1–β-TrCP1. Skp1 is purple, Skp2 is green, Skp1 is orange, and β-TrCP1 is yellow. The secondary structure elements for Skp1 and Fbs1 are labeled with black and red letters, respectively. (*B*) Close-up view of the interface between Skp1 and Fbs1 showing intermolecular contacts. Fbs1 is red and Skp1 is blue.

underlying the ubiquitination of N-glycoproteins by the SCF^{Fbs1} ubiquitin ligase, however, is unknown at present. To understand the mechanistic details of the SCF^{Fbs1}-mediated ubiquitination reaction, we determined the crystal structures of the SBD–glycoprotein and Skp1–Fbs1 complexes.

Results

Overall Structure of the Skp1–Fbs1 Complex. The Skp1–Fbs1 complex has an overall L-shaped structure with Skp1 and the Fbs1 subunits oriented ≈90° to each other (Fig. 1). Skp1 and the chitobiose-binding site (17) are located at the opposite ends of Fbs1. Fbs1 consists of four distinct domains: the PEST domain (residues 1–54), the F-box domain (residues 55–95), a linker domain (residues 96–124), and the SBD (residues 125–297). The electron densities of the N-terminal PEST domain (residues 1–47) and part of the linker domain (residues 104–108) are not visible, suggesting that these regions are flexible. Although the Skp1–Fbs1 complex was crystallized in the presence of 30 mM chitobiose, the chitobiose molecule is not visible in this structure. The F-box domain comprises four α helices, which is the same structural motif observed in the Skp1-binding domains of Skp2 and β-TrCP1 (Fig. 2*A*). The SBD in the Skp1–Fbs1 complex is composed of a 10-stranded antiparallel β-sandwich, and it can be superposed on the previously reported structure of SBD alone with an average rms deviation of 0.39 Å for the C^{α} atoms, indicating that the structures are very similar. On the other hand, the C-terminal linker helix α5 assumes slightly different positions in the two structures because of crystal packing and the flexibility of the linker domain, which consists of α5 and a loop structure.

The Skp1 in the Skp1–Fbs1 complex adopts the same BTB/POZ fold (18) observed in previously reported structures of Skp1 (7–9). Interestingly, the C-terminal α-helix α8 of previously reported structures of Skp1 complexed with other F-box proteins is replaced with an extended structure (C loop: residues 146–155) (Fig. 2*A*). The differences in the secondary structure of Skp1 may reflect different roles of the protein. With the exception of the C-terminal loop, the overall structure of Skp1 is almost identical to those of the protein in the Skp1–Skp2 and Skp1–β-TrCP1 complexes (rms deviations for the C^{α} atoms: 1.8 and 2.1 Å, respectively).

Skp1–F-Box Interface. Whereas the F-box domain of Fbs1 contains the same four-helix (α1–α4) structure seen in the domains of

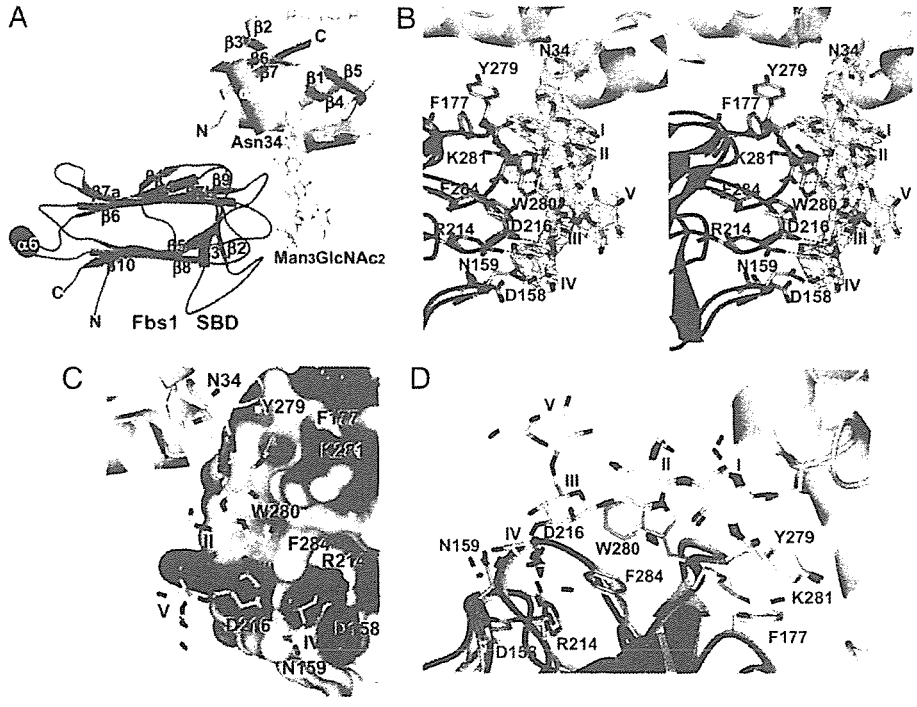

Fig. 3. Structure of the SBD–RNaseB complex. (*A*) The SBD is red and RNaseB is cyan. The secondary structure elements of the SBD and RNaseB are labeled. (*B*) Stereo view of the interface between the substrate-binding pocket of the SBD and the sugar of RNaseB. The $Man_3GlcNAc_2$ was modeled with the electron density map ($2F_o - F_c$ omit map of $Man_3GlcNAc_2$) contoured at 1.1 rms deviation. Fbs1 is red and RNaseB is cyan. (*C*) Surface representation of the substrate-binding pocket of the SBD bound to $Man_3GlcNAc_2$. The surface is colored according to the electrostatic potential of the residues (blue, positive; red, negative). (*D*) Comparison between the substrate-binding sites of the Fbs1 SBD (green) bound to chitobiose (yellow) and the Fbs1 SBD (red) bound to glycosylated RNaseB (cyan).

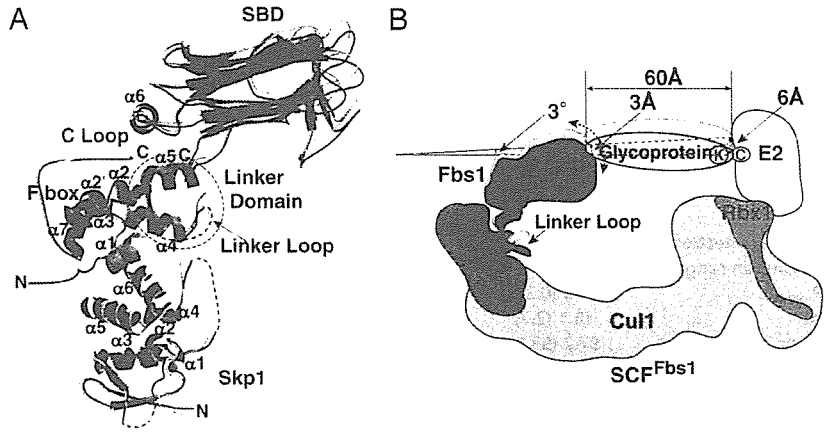

Fig. 4. Regulatory mechanism of SCF^{Fbs1} glycoprotein ubiquitination. (*A*) Comparison of the two crystal structures of the Skp1–Fbs1 complex. Skp1 (form 1), Fbs1 (form 1), Skp1 (form 2), and Fbs1 (form 2) are blue, red, yellow, and green, respectively. (*B*) Schematic representation of the model for ubiquitination on SCF^{Fbs1}. The E2 active-site cysteine and acceptor lysine residues are depicted with circled letters.

Skp2 (1.5-Å rms deviation for 27 C^{α} atoms) and β-TrCP1 (1.7-Å rms deviation for 28 C^{α} atoms), there are several differences. Helix α2 in Fbs1 is composed of two segments (α2 and α2′) separated by a turn, which causes it to bulge into the C loop of Skp1. The orientations of helices α3 and α4 of Fbs1 are similar to those of Skp2 but not to those of β-TrCP1 (Fig. 2*A*). Moreover, whereas the C-terminal region of the F-box domain of Skp2 is a loop structure, those of Fbs1 and β-TrCP1 form α-helices (α4).

The binding mode between Skp1 and the F-box domain of Fbs1 is almost identical to those between Skp1 and Skp2 (1.0-Å rms deviation for 120 C^{α} atoms) and between Skp1 and β-TrCP1 (1.1-Å rms deviation for 117 C^{α} atoms), except that the C loop of Skp1 interacts with the F-box domain through van der Waals contacts (Phe-145, Glu-149, Glu-150, Ala-151, Gln-152, and Val-153 of Skp1 interact with Val-72, Gln-73, Arg-76, Leu-77, and Leu-80 of Fbs1) (Fig. 2*B*). The positions of the Fbs1 F-box domain and α7 in Skp1 are shifted away from the N-terminal domain of Skp1 by ≈4.0 Å (Skp1–Skp2) or ≈2.5 Å (Skp1–β-TrCP1). These differences in the distances from the F-box domains to α7 of Skp1 and the C-terminal structures of Skp1 are likely due to the F-box structure.

Structure of the Glycoprotein Complex of the SBD. Ribonuclease B (RNaseB) is a glycoprotein that has a single high-mannose oligosaccharide ($Man_{6-8}GlcNAc_2$) attached at Asn-34 (19). RNaseB binds to the edge of the β-sandwich of the SBD (Fig. 3*A*). Clear electron density demonstrates the presence of $Man_3GlcNAc_2$ bound to the Fbs1 monomer, but the outer branches of the carbohydrate are disordered and not visible in the electron density map. The structure of the Fbs1-bound RNaseB, which consists of three α-helices and seven β-strands, is essentially identical to the previously reported structures of apo-RNaseB (20, 21); these structures have an average 0.59-Å rms deviation for the C^{α} positions. Similarly, the SBDs in the structures of the Skp1–Fbs1 and SBD–RNaseB complexes can be superposed with an average 0.48-Å rms deviation for the C^{α} positions, indicating that RNaseB binding does not cause any significant structural changes in the SBD.

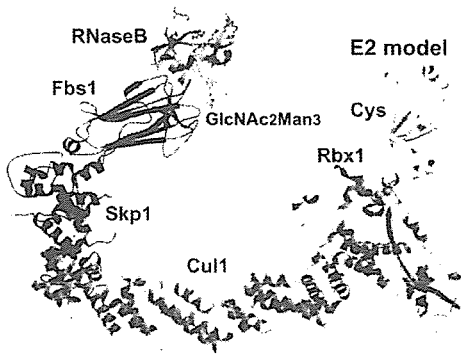

Fig. 5. Model of the SCF^{Fbs1}–RNaseB complex bound to E2. Cul1, Rbx1, Skp1, Fbs1, RNaseB, and E2 are green, orange, blue, red, cyan, and yellow, respectively. Lysine residues on the RNaseB surface are presented in ball-and-stick format and are coral.

Glycoprotein Recognition by the SBD in the SBD–RNaseB Complex. The sugar-binding surface consists of the four loops between β2 and β3, β3 and β4, β5 and β6, and β9 and β10. $Man_3GlcNAc_2$ interacts with nine Fbs1 residues (Asp-158, Asn-159, Phe-177, Arg-214, Asp-216, Tyr-279, Trp-280, Lys-281, and Phe-284) through hydrogen bonds and/or van der Waals contacts (Fig. 3 *B* and *C*). The molecular recognition mechanism between the chitobiose moiety and the amino acid residues in Fbs1 is similar to that reported previously for the SBD–chitobiose complex (17). The methyl group of the *N*-acetyl moiety from the GlcNAc (I) residue is inserted into a small hydrophobic pocket surrounded by the side chains of Phe-177, Tyr-279, and Lys-281; and the O3 atom forms a hydrogen bond with the main chain N atom of Lys-281. The GlcNAc (II) residue is stacked on the aromatic ring of Trp-280 and the O6 atom forms a hydrogen bond with the carbonyl oxygen atom of Lys-281. The two GlcNAc residues form an intramolecular hydrogen bond between the O3 atom of GlcNAc (I) and the O6 atom of GlcNAc (II). Formation of these hydrogen bonds fixes the orientation of the β(1→4)-linked GlcNAc residues. Comparison of the SBD–RNaseB complex and the previously reported SBD–chitobiose complex reveals that the substrate binding pockets (Phe-177, Tyr-279, Trp-280, and Lys-281) and the chitobiose structures can be superposed with an average rms deviation of 0.69 Å for all of the atoms (Fig. 3*D*). Only the side chain of Lys-281 has a different conformation, and it has been shown that Lys-281 is not essential for the binding to chitobiose (17). The outer mannose-binding residues of the SBD also do not exhibit significant conformational changes. We have reported that Fbs1 recognizes not only chitobiose but also the outer mannose branches (17). The O4 atom of Man(III)

BIOCHEMISTRY

Table 1. Data collection, phasing, and refinement statistics

	Skp1–Fbs1	Skp1–Fbs1/Thimerosal	Skp1–Fbs1	SBD–RNaseB
Data collection				
Space group	$P3_221$	$P3_221$	$P2_12_12_1$	$P432$
Cell parameters, Å				
a	106.7	106.6	66.2	148.6
b	106.7	106.6	111.1	148.6
c	110.2	113.7	153.3	148.6
Unique reflections	27,964	17,765	12,269	15,839
Resolution range, Å	2.40 (2.49–2.40)	2.80 (2.90–2.80)	3.50 (3.63–3.50)	2.70 (2.80–2.70)
R_{merge}	0.045 (0.327)	0.058 (0.328)	0.103 (0.225)	0.078 (0.325)
$I/\sigma I$	18.1 (2.7)	16.0 (2.2)	7.0 (4.1)	13.9 (5.2)
Completeness, %	97.7 (93.0)	95.7 (79.6)	85.2 (79.0)	99.4 (97.9)
Redundancy	5.4 (2.9)	6.2 (2.3)	2.6 (2.1)	11.8 (6.4)
Refinement				
No. of reflections	26,521		12,279	15,049
R_{work}/R_{free}	0.233/0.291		0.223/0.299	0.216/0.288
rms deviations				
Bond lengths, Å	0.010		0.022	0.026
Bond angles, °	1.33		2.08	2.51

Values in parentheses represent the highest-resolution shell.

forms a hydrogen bond with the sidechain O^{δ} atom of the Asp-216 sidechain; this hydrogen bond stabilizes the complex with the Manβ(1→4)GlcNAc$_2$ moiety. Clear electron density is observed between the β(1→4)-linked Man residue and Asp-216 in Fbs1. Furthermore, Asp-216 is conserved in other F-box proteins that contain an F-box-associated domain, suggesting that it plays a role in the recognition of oligosaccharides. Man(IV) forms hydrogen bonds with the sidechain N^{δ} atom of Asn-159 through the O2 atom and with the sidechain N^{η} atom of Arg-214 through the O5 atom. On the other hand, Man(V) protrudes from the binding site and does not interact with Fbs1. These results indicate that the GlcNAc$_2$ core, β(1→4)-linked Man(III), and α(1→3)-linked Man(IV) play significant roles in the binding to Fbs1. Whereas Man$_8$GlcNAc$_2$ is thought to be the major N-glycan among unfolded glycoproteins that are translocated into the cytosol for endoplasmic reticulum-associated degradation, our results indicate that Man$_3$GlcNAc$_2$ can be sufficiently recognized by the SCF^{Fbs1} complex. Indeed, various synthetic oligosaccharides were used to show that Man$_3$GlcNAc$_2$ and Man$_8$GlcNAc$_2$ have similar affinities for Fbs1 (22). On the other hand, the binding affinities of Man$_8$GlcNAc$_1$ and chitobiose for Fbs1 are several orders of magnitude lower than those of Man$_3$GlcNAc$_2$ and Man$_8$GlcNAc$_2$, indicating that Man$_3$GlcNAc$_2$ is required for efficient binding to Fbs1 (15, 22). Moreover, the binding site provides substrate selectivity and specificity based on its shape and hydrogen-bonding network.

There are limited contacts between the SBD and RNaseB; the interface involves only 514 Å^2 of surface-accessible area. The surface areas occupied by Man$_3$GlcNAc$_2$ and the protein portion of the substrate are 349 and 165 Å^2, respectively. In addition to the smaller contact area, the protein portion of RNaseB does not form a hydrogen bond with Fbs1, suggesting that Man$_3$GlcNAc$_2$, but not the protein in RNaseB, defines the interaction with Fbs1.

Linker Flexibility Might Accommodate a Range of Substrates. Two crystal forms were identified for Skp1–Fbs1 ($P3_221$ and $P2_12_12_1$ define form 1 and form 2, respectively). These two forms have essentially the same overall structure (rms deviation of 1.1 Å for the C^{α} atoms) (Fig. 4*A*). Whereas the Skp1 proteins are well aligned with each other, the SBD of Fbs1 in form 2 is tilted farther away from Skp1 by ≈3°. The 3° tilt angle of the SBD creates a 3-Å gap at the substrate-binding site and a 6-Å shift at the E2 active site. This flexibility seems to be due in part to the linker-domain structure of Fbs1 (Fig. 4*A*). Residues 100–103 and 113–115 are shifted significantly compared with form 1. Although the linkage between the F-box and WD40 domains does not seem to be exceedingly rigid in the yeast Cdc4 structure, deletion of helix α5 or the lengthening of helix α6 due to an insertion of amino acid residues disrupts Cdc4 function *in vivo*, suggesting that the orientation and rigidity of the linkage between the F-box and the substrate-binding domains is important for SCF function (8). In the structure of Fbs1, the interaction between α5 and the linker loop through van der Waals contacts (His-113 of the linker loop to Gln-115, Phe-119, and Arg-123 of α5) is not rigid, and residues 104–108 of the linker domain are not visible in the electron density map. This structure indicates that the linkage between the F-box domain and the SBD of Fbs1 is somewhat flexible. This feature might allow the protein to accommodate a range of substrates (Fig. 4*B*).

Discussion

In this study, we determined the crystal structures of two crystal forms of the Skp1–Fbs1 complex and the SBD–RNaseB complex at 2.4-, 3.5-, and 2.7-Å resolutions, respectively. The structure of the Skp1–Fbs1 complex illustrates a different class of F-box proteins within the SCF ubiquitin ligase model. A model of the SCF^{Fbs1}–RNaseB–E2 complex was generated simply by superposition of the Skp1 subunits from the Skp1–Fbs1 and Skp1–Cul1–Rbx1 structures (PDB ID code 1LDK), the RING-finger domains derived from Rbx1 and from the c-Cbl subunit of the c-Cbl-UbcH7 structure (PDB ID code 1FBV) (23), the E2 subunits of the c-Cbl-UbcH7 structure, and the SBD-RNaseB structure. In this SCF^{Fbs1}-RNaseB model, RNaseB points toward the E2-binding site on Rbx1 (Fig. 5). The distance between the E2 active-site cysteine and the substrate-binding site is ≈60 Å, which is similar to the value that was reported previously (7, 8, 10). Despite differences in the sizes of the substrates and the positions of ubiquitinated lysine residues, the distance between the E2 active-site cysteine and the substrate-binding site is conserved among the SCF complexes. The same mechanism that allows the E2 active-site cysteine to reach the ubiquitinated lysine residues of the substrates is used independently of the type of F-box protein.

In the case of RNaseB, the distances between the E2 active-site cysteine and the lysine residues in RNaseB are 58.6–88.4 Å in the model of the SCF^{Fbs1}–RNaseB–E2 complex, whereas the

lysine residues in RNaseB are between 5.3 and 36.9 Å away from Asn-34. RNaseB is smaller than the minimum distance required to reach E2. Actually, SCF^{Fbs1} was not able to ubiquitinate RNaseB *in vitro*. This could be because RNaseB is too small, the lysine residues are at the wrong positions, or RNaseB is fixed because of contacts between $Man_3GlcNAc_2$ and Fbs1.

One of the most important properties for ubiquitination is the rigidity of the SCF–ubiquitin–ligase complex structure, because it serves to correctly position the target protein and E2. The two crystal structures of the Skp1–Fbs1 complex described in the present study, however, show differences in the orientation of the SBD. We propose that SCF^{Fbs1} has the ability to nonspecifically ubiquitinate glycoproteins targeted to the endoplasmic reticulum-associated degradation pathway. The protein portion of a target glycoprotein bound to Fbs1 may rotate at the linkage site between the innermost GlcNAc moiety and the asparagine residue, and the acceptor lysine residue can be located at a variety of positions. In SCF^{Fbs1}, the relative motion of the linker domain between the F-box domain and the SBD might be necessary to accommodate the different positions of the acceptor lysine residues in the various endoplasmic reticulum-associated degradation substrates.

SCF^{Fbs1} is a functionally unique molecule that recognizes the innermost $Man_3GlcNAc_2$ in N-glycans as a marker of denatured proteins. Our results provide a mechanistic basis for the recognition and ubiquitination of various glycoproteins by SCF^{Fbs1}.

Materials and Methods

Protein Expression and Purification. The Skp1–Fbs1 complex was coexpressed from the pET28b plasmid (Novagen, Madison, WI) in BL21 (DE3) cells. Full-length Skp1 was expressed as a 6× His-tagged protein, and full-length Fbs1 was expressed as an untagged protein. The complex was purified stepwise by Ni affinity, anion exchange, and gel-filtration chromatography. The Skp1–Fbs1 complex was then concentrated to ≈10 mg/ml by ultrafiltration in 25 mM Tris·HCl (pH 7.5) and 1 mM DTT.

For the SBD–RNaseB complex (with SBD residues 105–297 of Fbs1), the SBD and RNaseB (Sigma, St. Louis, MO) were combined in a 1:1 molar ratio and purified by gel-filtration chromatography. Fractions containing the SBD–RNaseB complex were then concentrated to ≈10 mg/ml and used for crystallization.

Crystallization and Data Collection. Crystals of Skp1–Fbs1 and SBD–RNaseB were obtained at 20°C by using the sitting-drop vapor diffusion method. Skp1–Fbs1 crystals were grown from 2.0 M ammonium sulfate, 0.1 M sodium citrate (pH 5.7), and 30 mM chitobiose, which produced two crystal forms. The SBD–RNaseB crystals were prepared by using 2.0% (vol/vol) PEG 400, 0.1 M Hepes (pH 7.5), and 2.1 M ammonium sulfate.

Diffraction data sets for Skp1–Fbs1 and SBD–RNaseB were collected at beamline BL44XU (SPring-8, Hyogo, Japan). Data processing and reduction were carried out with the HKL program suite (24). The two crystal forms of Skp1–Fbs1 and the SBD–RNaseB crystals belong to the $P3_221$ (Skp1–Fbs1 form 1), $P2_12_12_1$ (Skp1–Fbs1 form 2), and $P432$ (SBD–RNaseB) space groups. Heavy-atom soaks of the Skp1–Fbs1 crystals (form 1) were performed in crystallization buffer with 1 mM thimerosal for 5 min. Data collection, phasing, and refinement statistics are summarized in Table 1.

Structure Determination and Refinement. The structure of Skp1–Fbs1 was determined by a combination of molecular replacement, single isomorphous replacement, and anomalous scattering with an Hg derivative. The initial single isomorphous replacement and anomalous scattering phases were calculated with SHARP (25) and then improved by density modification with DM (26). Molecular replacement with the program MOLREP (27) was used to locate the Skp1 and SBD portions of the complex with search models consisting of Skp1 from SCF (PDB ID code 1LDK) and the SBD of Fbs1 (PDB ID code 1UMH). The model was further built with the program COOT (28) and then was improved by several cycles of manual rebuilding and refinement with the program REFMAC5 (29). The structure of crystal form 2 was solved by molecular replacement using MOLREP with the refined model of form 1.

The structure of SBD–RNaseB was determined by using the molecular replacement technique, MOLREP, and the structures of the SBD and RNaseB. The refined model contains residues 123–297 of the SBD and residues 1–124 of RNaseB. Phasing and refinement statistics are summarized in Table 1. There are no residues in disallowed regions of the Ramachandran plot. Structure figures were generated by using MOLSCRIPT (30), RASTER3D (31), and CCP4MG (32).

We thank Tomitake Tsukihara for helpful advice and stimulating discussions at all stages of the x-ray crystallographic analysis and the members of beamline BL44XU for help during the data collection at SPring-8. This work was supported in part by Grant-in-Aid for Scientific Research in Priority Areas 18054011 from the Ministry of Education, Culture, Sports, Science, and Technology (Japan).

1. Hershko A, Ciechanover A, Varshavsky A (2000) *Nat Med* 6:1073–1081.
2. Sherman MY, Goldberg AL (2001) *Neuron* 29:15–32.
3. Pickart CM (2001) *Annu Rev Biochem* 70:503–533.
4. Deshaies RJ (1999) *Annu Rev Cell Dev Biol* 15:435–467.
5. Jin J, Cardozo T, Lovering RC, Elledge SJ, Pagano M, Harper JW (2004) *Genes Dev* 18:2573–2580.
6. Yoshida Y (2003) *J Biochem (Tokyo)* 134:183–190.
7. Wu G, Xu G, Schulman BA, Jeffrey PD, Harper JW, Pavletich NP (2003) *Mol Cell* 11:1445–1456.
8. Orlicky S, Tang X, Willems A, Tyers M, Sicheri F (2003) *Cell* 112:243–256.
9. Schulman BA, Carrano AC, Jeffrey PD, Bowen Z, Kinnucan ER, Finnin MS, Elledge SJ, Harper JW, Pagano M, Pavletich NP (2000) *Nature* 408:381–386.
10. Zheng N, Schulman BA, Song L, Miller JJ, Jeffrey PD, Wang P, Chu C, Koepp DM, Elledge SJ, Pagano M, *et al.* (2002) *Nature* 416:703–709.
11. Hao B, Zheng N, Schulman BA, Wu G, Miller JJ, Pagano M, Pavletich NP (2005) *Mol Cell* 20:9–19.
12. Ellgaard L, Helenius A (2003) *Nat Rev Mol Cell Biol* 4:181–191.
13. Erhardt JA, Hynicka W, DiBenedetto A, Shen N, Stone N, Paulson H, Pittman RN (1998) *J Biol Chem* 273:35222–35227.
14. Yoshida Y, Chiba T, Tokunaga F, Kawasaki H, Iwai K, Suzuki T, Ito Y, Matsuoka K, Yoshida M, Tanaka K, *et al.* (2002) *Nature* 418:438–442.
15. Yoshida Y, Tokunaga F, Chiba T, Iwai K, Tanaka K, Tai T (2003) *J Biol Chem* 278:43877–43884.
16. Yoshida Y, Adachi E, Fukiya K, Iwai K, Tanaka K (2005) *EMBO Rep* 6:239–244.
17. Mizushima T, Hirao T, Yoshida Y, Lee SJ, Chiba T, Iwai K, Yamaguchi Y, Kato K, Tsukihara T, Tanaka K (2004) *Nat Struct Mol Biol* 11:365–370.
18. Aravind L, Koonin EV (1999) *J Mol Biol* 285:1353–1361.
19. Liang CJ, Yamashita K, Kobata A (1980) *J Biochem (Tokyo)* 88:51–58.
20. Williams RL, Greene SM, McPherson A (1987) *J Biol Chem* 262:16020–16031.
21. Ko TP, Williams R, McPherson A (1996) *Acta Crystallogr D* 52:160–164.
22. Hagihara S, Totani K, Matsuo I, Ito Y (2005) *J Med Chem* 48:3126–3129.
23. Zheng N, Wang P, Jeffrey PD, Pavletich NP (2000) *Cell* 102:533–539.
24. Otwinowski Z, Minor W (1997) *Methods Enzymol* 276:307–326.
25. Bricogne G, Vonrhein C, Flensburg C, Schiltz M, Paciorek W (2003) *Acta Crystallogr D* 59:2023–2030.
26. Collaborative Computational Project 4 (1994) *Acta Crystallogr D* 50:760–763.
27. Vagin AA, Teplyakov A (1997) *J Appl Crystallogr* 30:1022–1025.
28. Emsley P, Cowtan K (2004) *Acta Crystallogr D* 60:2126–2132.
29. Murshudov GN, Vagin AA, Dodson EJ (1997) *Acta Crystallogr D* 53:240–255.
30. Kraulis PJ (1991) *J Appl Crystallogr* 24:946–950.
31. Merritt EA, Murphy ME (1994) *Acta Crystallogr D* 50:869–873.
32. Potterton E, McNicholas S, Krissinel E, Cowtan K, Noble M (2002) *Acta Crystallogr D* 58:1955–1957.

Cell Death and Differentiation (2007), 1–8

www.nature.com/cdd

Review

Constitutive autophagy: vital role in clearance of unfavorable proteins in neurons

M Komatsu[1,2,3], T Ueno[1], S Waguri[4], Y Uchiyama[5], E Kominami[1] and K Tanaka*[,2]

Investigations pursued during the last decade on neurodegenerative diseases have revealed a common mechanism underlying the development of such diseases: conformational disorder of certain proteins leads to the formation of misfolded protein oligomers, which subsequently develop into large protein aggregates. These aggregates entangle other denatured proteins and lipids to form disease-specific inclusion bodies. The failure of the ubiquitin-proteasome system to shred the protein aggregates has led investigators to focus their attention to autophagy, a bulk degradative system coupled with lysosomes, which is involved in non-selective shredding of large amounts of cytoplasmic components. Research in this field has demonstrated the accumulation of autophagic vacuoles and intracytoplasmic protein aggregates in patients with various neurodegenerative diseases. Although autophagy fails to degrade large protein aggregates once they are formed in the cytoplasm, drug-induced activation of autophagy is effective in preventing aggregate deposition, indicating that autophagy significantly contributes to the clearance of aggregate-prone proteins. The pivotal role of autophagy in the clearance of aggregate-prone proteins has been confirmed by a deductive approach using a brain-specific autophagy-ablated mouse model. In this review, we discuss the consequences of autophagy deficiency in neurons.
Cell Death and Differentiation advance online publication, 2 March 2007; doi:10.1038/sj.cdd.4402120

Cell proteins exist in a balance between continuous synthesis and degradation. In general, this flow of synthesis and degradation (i.e., turnover) contributes to exertion of cell-type-specific functions and maintenance of cell homeostasis. However, it is not uncommon that living cells are exposed to various environmental stresses, such as oxygen radicals and UV irradiation. Unfortunately, these stresses frequently cause various types of protein injuries that vitiate normal cellular functions or homeostasis and may eventually cause cell death. Prompt elimination of injured harmful proteins, which is particularly important in non-proliferative cells, such as neurons, is totally dependent on proper function of protein catabolic machineries, in which two major sophisticated apparatuses play principal roles. One is the proteasome, which is an elegantly organized multi-protease complex with catalytic activities inside its central proteinaceous chamber. It plays crucial roles in selective degradation of short-lived regulatory proteins as well as proteins with aberrant structures that should be eliminated from the cells.[1] The other apparatus is the lysosome that contains many acidic hydrolases, which are separated from the cytosol by the limiting membrane. In this lysosomal pathway, degradation of plasma membrane proteins and extracellular proteins is mediated by endocytosis, whereas that of cytoplasmic components is achieved through distinct types of autophagic pathways; for example, macroautophagy, microautophagy, and chaperone-mediated autophagy.[2,3]

Macroautophagy (hereafter referred to as autophagy), the major type of autophagy, is the bulk protein degradation pathway associated with marked membrane dynamics. In response to various stimuli, such as starvation (i.e., nutritional step-down) and humoral (trophic) factors (e.g., glucagon and cytokines), an isolation membrane appears promptly in the cytosol, where it gradually elongates to sequestrate cytoplasmic constituents. Subsequently, the edges of the membrane fuse together to form double-membrane structures termed autophagosomes. Autophagosomes rapidly fuse with lysosomes, and their contents engulfed together with the inner membrane are degraded by a variety of lysosomal digestive hydrolases (Figure 1).[4] In addition to the importance of starvation-induced (i.e., adaptive) autophagy equipped as a fundamental survival strategy in all eukaryotic cells, growing lines of evidence point to the importance of basal autophagy that operates constitutively at low rate even under nutrient-rich environment and to its key role in global turnover of cellular components including organelles.

[1]Department of Biochemistry, Juntendo University School of Medicine, Tokyo, Japan; [2]Laboratory of Frontier Science, Tokyo Metropolitan Institute of Medical Science, Tokyo, Japan; [3]PRESTO, Japan Science and Technology Corporation, Kawaguchi, Japan; [4]Department of Anatomy and Histology, Fukushima Medical University School of Medicine, Fukushima, Japan and [5]Department of Cell Biology and Neurosciences, Osaka University Graduate School of Medicine, Osaka, Japan
*Corresponding author: K Tanaka, Laboratory of Frontier Science, Tokyo Metropolitan Institute of Medical Science, Bunkyo-ku, Tokyo 113-8613, Japan.
Tel/Fax: +81 3 3823 2237; E-mail: tanakak@rinshoken.or.jp
Keywords: autophagy; neurodegenerative diseases; ubiquitin; knockout-mice; Atg7
Abbreviations: AD, Alzheimer's disease; APP, amyloid precursor protein; Aβ, beta-amyloid; GFP, green fluorescent protein; HD, Huntington's disease; LC3, microtubule-associated protein 1 light chain 3/MAP1LC3; mTor, mammalian target of rapamycin; PD, Parkinson's disease; PS1, presenilin-1; SDH, succinate dehydrogenase; TCA, tricarboxylic acid
Received 28.11.06; revised 05.2.07; accepted 05.2.07; Edited by E Baehrecke

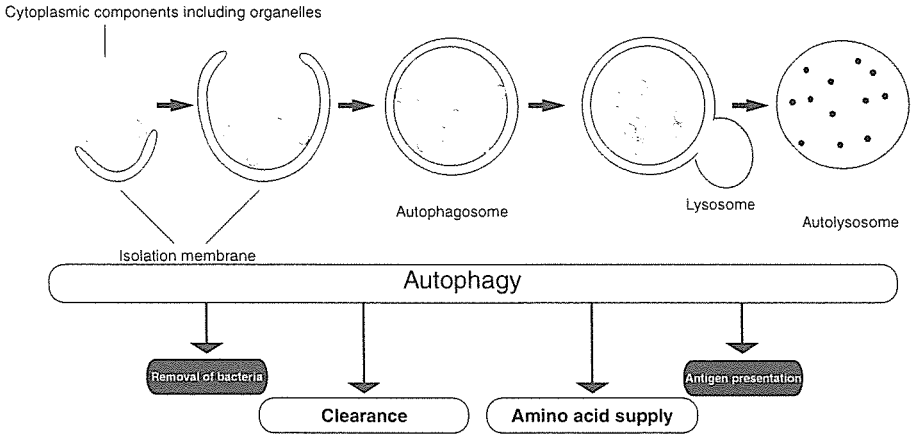

Figure 1 Schematic representation of the physiological functions of autophagy. Autophagy is induced in response to emergency states such as nutrient starvation or bacterial infection, which results in the degradation of cytoplasmic components for amino-acid supply (non-selective process) and the removal of bacteria that invade the cytoplasm (selective process). Autophagy also contributes to processing viral proteins such as EBNA1 and certain cytosolic proteins (e.g., tumor antigens) for presentation onto major histocompatibility complex (MHC) class II molecules. Autophagy also occurs constitutively even under a nutrient-rich state and contributes to global turnover of cellular components. It is an essential cellular process that maintains homeostasis in quiescent cells (e.g., hepatocytes and neurons)

Starvation-induced Autophagy

The most fundamental function of autophagy is cellular adaptation to nutritional stress. In yeast, autophagy is promptly induced upon nitrogen starvation.[5] Transgenic mice overexpressing GFP (green fluorescent protein)-LC3 is an interesting animal model for monitoring autophagy.[6] LC3 (microtubule-associated protein 1 light chain 3/MAP1LC3), originally identified as a small subunit of MAP-1A/MAP-1B, is processed by Atg4B protease to expose the carboxyl-terminal glycine whose residue serves as a donor site for conjugation of target molecules.[7–9] The processed form (LC3-I) undergoes two consecutive ubiquitylation-like modification reactions catalyzed by Atg7 (E1, activating-like enzyme) and Atg3 (E2, conjugating-like enzyme), to be covalently coupled with phosphatidylethanolamine (PE).[10–12] The PE-conjugated form, designated as LC3-II, is then recruited to autophagosomal membrane. Thus, LC3-II is a promising marker for autophagosomal membranes.[7] Similar to endogenous LC3, GFP-LC3 responds to nutrient-starved conditions to form GFP-LC3-II, which is recruited to autophagosomes in GFP-LC3 transgenic mice.[6] The autophagosomal GFP-LC3-II could be detected as dots in fluorescence microscopic analyses. Under fasting conditions, the numbers of fluorescent dots increase in the cytoplasm of the liver, heart, and skeletal muscles of GFP-LC3 transgenic mice.

Starvation-induced protein degradation has been best investigated in the liver. One unequivocal characteristic of hepatic protein degradation is its dependence on the nutrient conditions. Depending on the dietary cycle of the animal, the rate of protein degradation fluctuates between ~1.5% (fed state) and ~4.5% (fasted state) of total liver proteins per hour.[13] Recently, we generated *Atg7*$^{F/F}$:Mx1 mice in which autophagy could be successfully inactivated in the livers.[14] Whereas the amount of total liver proteins decreased to about 66% in the control liver by 1-day fasting, fasting did not result in a significant decrease in the amount of total proteins in the autophagy-deficient liver, indicating that the decrease in total proteins upon fasting is indeed dependent on autophagy. Measurement of the activity of mitochondrial enzyme, succinate dehydrogenase (SDH), showed that fasting was also associated with a significant decrease in SDH activity in total extracts in the control livers, and such reduction was proportional with the decrease in the amount of total protein. On the other hand, fasting was not associated with any change in SDH activity in the autophagy-deficient livers. These results suggest that the mitochondria and cytoplasmic proteins are proportionally degraded upon fasting by autophagy. Thus, it is plausible that autophagosomes surround cytoplasmic components including mitochondria at random to adapt for starvation.

Yeast deficient in autophagy rapidly dies under nutrition-poor conditions,[15] suggesting the important roles of autophagy in maintaining nutrient supply. Indeed, newborn mice deficient in Atg5 or Atg7, which are indispensable for autophagosome formation, show poor response to starvation with regard to production of amino acids, and die within the first day of life.[14,16] Furthermore, Lum *et al.*[17] reported that in IL-3-dependent cells, which cannot undergo apoptosis due to knockout of both Bax and Bak, impairment of autophagy leads to rapid cell death by loss of IL-3, and such death is suppressed by addition of methylpyruvate, a TCA (tricarboxylic acid) substrate. These results suggest that one of the important roles of autophagy is the supply of amino acids under nutrient-poor environment (Figure 2, top panel).

Unique Features of Neuronal Autophagy

The brain appears to be a specially protected tissue where nutrients (e.g., amino acids, glucose, and ketone bodies) are compensated by constant supply from other organs even under starvation conditions and consequently autophagy does not operate in response to nutritional stress. Indeed, autophagosomes-related GFP-LC3 dots do not increase at all

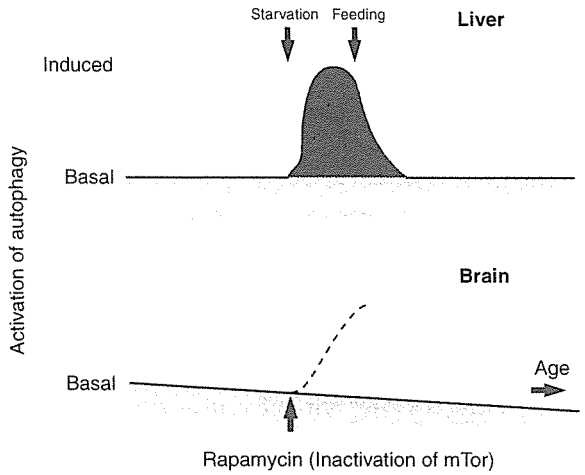

Figure 2 Schematic presentation of induced autophagy and basal (constitutive) autophagy. Under nutrient-rich conditions, autophagic proteolysis proceeds in hepatocytes at a basal rate (top panel, pink zone), which is enhanced two- to threefold to an induced rate under nutrient-starvation conditions (blue zone). When animals are re-fed, the rate of autophagic proteolysis promptly returns to the basal level. In contrast to the liver, autophagy in the brain is thought to proceed at a basal rate, irrespective of nutrient conditions. However, this basal or constitutive autophagy plays a critical role in the quality control system of neurons. Rapamycin and its homologs, which upregulate autophagy to an induced level (bottom panel, broken line), are expected to prevent the accumulation of aggregate-prone proteins. It should be noted that autophagic activity declines with age, which may relate to the age-dependent onset of neurodegenerative diseases

in the brain of GFP-LC3 transgenic mice, irrespective of fasting.[6] A reasonable conclusion drawn from these observations is that autophagy in the brain proceeds at a basal rate but is not enhanced under fasting conditions (Figure 2, bottom panel). Another peculiar feature of autophagy in neurons is the free localization of autophagosomes in the cytoplasm but the restriction of lysosomes mainly to the juxtanuclear cytoplasm of the cell body in the neuron. This feature means that autophagosomes formed in dendrites and synaptic terminal regions must be transported to the lysosome in the cell body. A previous kinetic analysis of organelle movements in cultured neurons indicated that phase-dense vesicles, containing sequestered cytoplasmic proteins and materials taken up by endocytosis, move along microtubules in the axon to the lysosomes in the cell body.[18] These data suggest that fusion of autophagosomes formed in the synaptic cytoplasm with lysosomes is strictly dependent on retrograde axonal transport. It has been reported that mutations of dynein and dynactin in mice and human cause motor neuron degeneration resembling amyotrophic lateral sclerosis.[19,20] Using cultured PC12 cells, flies and mice expressing different kinds of aggregate-prone proteins, such as expanded polyQ and mutant α-synuclein, Ravikumar *et al.*[21] demonstrated that inhibition of dynein function retarded the clearance of aggregates by inhibiting autophagosome-lysosome fusion. It has been shown recently that aggregate-prone proteins formed in the cytoplasm of cultured HeLa cells and a cultured neural cell line, are degraded by autophagy, which is also dependent on intact microtubules.[22]

Autophagic Vacuoles in Neurodegenerative Diseases

Morphological analyses revealed that accumulation of abnormally large number of autophagic vacuoles (autophagosomes plus autolysosomes) or the appearance of irregularly shaped autophagic vacuoles is frequently observed as a common feature in many inherited neurodegenerative diseases.[23–27] Inclusion bodies, composed of ubiquitin-positive cytoplasmic remnants, and lipofuscin deposits, together with dispersed autophagic vacuoles and lysosomes are the primary hallmarks of the late stages of these diseases. Increased density of autophagic vacuoles seems to reflect enhanced autophagosome formation, on one hand, but their accumulation with blurred structures of sequestered materials in their lumen may also imply impaired autolysosomal degradation, on the other. In fact, these morphological features are not present in normal neurons and resemble those of cultured HEK293 cells that have been placed under starvation conditions in the presence of lysosomal proteinase inhibitors.[28] Under these conditions, autophagic response is markedly enhanced, but autophagic proteolysis is simultaneously inhibited. In addition, as observed in Danon disease, which is caused by mutation of the lysosome-associated membrane protein-2 (LAMP-2), and LAMP-2-deficient mice, impairment of autophagosome-lysosome fusion also leads to unequivocal increment of autophagosomes in cardiac muscles and hepatocytes.[29,30]

Autophagy in Alzheimer's, Huntington's, and Parkinson's Diseases

Protein conformational disorders, such as Alzheimer's disease (AD), Huntington's disease (HD), and Parkinson's disease (PD), are characterized by abnormally high accumulation of misfolded and/or unfolded proteins in the surviving neurons as detected at postmortem examination. In this section, we will evaluate the role of autophagy in those hereditary neurodegenerative diseases.

It has become clear that autophagy is linked to the pathogenesis of HD. HD is an autosomal dominant disorder caused by mutations of huntingtin, a cytosolic protein that has a polyglutamine (polyQ) tract in its N-terminus. In HD, abnormal expansion of polyQ caused by codon (CAG) reiterations in exon 1 of the Huntingtin gene produces mutated huntingtin with an expanded polyQ repeat (more than 37 polyQs). Mutant huntingtin with a longer polyQ tract has a stronger tendency than the wild type to form aggregates, both accelerating the onset and worsening the severity of the disease, suggesting that the progressive formation of insoluble polyQ aggregates is a key event leading to manifestation of the disease. Indeed, model mouse with mutant polyQ is associated with formation of nuclear and cytoplasmic inclusions in their neurons.[31] However, recent studies revealed that globular and protofibrillar intermediates form before the organization of mature huntingtin aggregates, and that these are toxic and could lead to disturbances of genetic transcription networks and mitochondrial dysfunctions.[32,33] Then, what are the mechanisms by which autophagy clears mutant huntingtin? Ultrastructural examination of huntingtin-transfected cells showed abundant accumulation of cathepsin

D-positive autophagic vacuoles with or without sequestered cellular constituents, dense lysosomes, and multilamellar and tubuloveseicular structures.[26] Ravikumar *et al.*[34] investigated whether autophagy can degrade mutant huntingtin with expanded polyQ repeats. Degradation of 74 polyQ repeats fused to the amino terminus of GFP (polyQ74-GFP) transfected into COS7 or PC12 cells was inhibited by 3-methyladenine, a specific inhibitor of autophagy, and enhanced by rapamycin. Rapamycin acts by inhibiting the mammalian target of rapamycin (mTor) kinase, which forms the core of a nutrient- and growth factor-sensitive complex that control protein synthesis, and suppresses autophagy.[35] Importantly, inhibitors of autophagy enhance cell death, whereas rapamycin prevents the effects. Furthermore, once the overexpressed polyQ74-GFP forms insoluble large aggregates, the insoluble aggregates become resistant to rapamycin-induced autophagy. The data clearly demonstrate that failure to degrade polyQ expansions by autophagy is associated with accelerated progression of HD and that stimulation of autophagy in the early stages of the disease by rapamycin treatment could prevent deposition of polyQ aggregates. Rapamycin enhances the autophagic clearance of different proteins with long polyQ and polyalanine (polyA)-expanded proteins, and reduces their neurotoxicity. Thus, rapamycin and its analogs can be potentially used therapeutically for neurodegenerative diseases caused by aggregate-prone proteins.[36] It has been shown that mTor is sequestered in polyQ aggregates in transgenic mice expressing mutant huntingtin and patient brains of HD. Sequestration of mTor in polyQ aggregates inhibits nuclear-cytoplasm shuttling of mTor, leading to inactivation of mTor.[37] The inactivation in turn induces autophagy. Hence, co-sequestration of aggregates with mTor leads to inhibition of mTor activity, which may provide a partial explanation for accumulation of autophagic vacuoles in neurodegenerative diseases. On the other hand, the activation of autophagy via an insulin signal pathway clears accumulated polyQ proteins independent of mTor, as reported by Yamamoto *et al.*[38] They found that aggregates of mutant huntingtin activate insulin receptor substrate-2 involving the signaling cascades of insulin and insulin-like growth factor 1. Such activation turns on class III PI3K to induce autophagy, thus contributing to clearance of huntingtin aggregates.[38]

Invariably, AD is the most prevalent form of neurodegenerative diseases with dementia and associates with extracellular deposition of beta-amyloid (Aβ). Presenilin-1 (PS1) is one of several proteins linked to early-onset familial AD, and together with PS2, plays a catalytic role in the γ-secretase complex necessary for intermediate proteolysis of the amyloid precursor protein (APP) followed by liberation of Aβ. Although it has been noticed that autophagic vacuoles accumulate in hippocampal and prefrontal cortical pyramidal neurons of Alzheimer-type dementia,[23,24] the mechanism remains unclear. Wilson *et al.*[39] found the formation of enlarged late endosome-like structures, including α- and β-synuclein, in the perikarya of PS1$^{-/-}$ primary neurons and hippocampal tissue of patients with the Levy body variant of AD. Formation of such organelles is rescued by exogenous expression of not only wild-type PS but also dominant-negative PS1 lacking its activity, indicating that PS1 has another function besides γ-secretase. Esselens *et al.*[40] demonstrated the accumulation of telencephalin, a neural specific intercellular adhesion molecule known to interact with PS1, in vacuoles positive for Atg12 and LC3, but not cathepsin D, in PS1$^{-/-}$ hippocampal neurons. Similar to the report of Wilson *et al*,[39] the formation of such vacuoles was suppressed by not only wild-type but also mutant PS1. Furthermore, Esselens *et al.*[40] used cathepsin D knockout mice to show the degradation of telencephalin in lysosomes. Collectively, these results suggest that PS1 might play important roles in autophagosome and lysosomal fusion step. Recently, Yu *et al.*[41] reported the role of autophagy in Aβ production. Their exhaustive electron and immunoelectron microscopic analyses revealed accumulation of LC3-positive autophagic vacuoles in brains of AD patients and in AD model mice, neural cell lines, and in a non-neural APP-expressing cell line, and also the localization of PS1, Aβ40, Aβ42, and necastrin on internal and limiting membrane components of autophagic vacuoles. Further, they found that induction of autophagy evoked Aβ production, and inversely, inhibition of autophagy suppressed Aβ production. Finally, they observed the PS1-dependent γ-secretase activity in biochemical isolated autophagic vacuoles. Based on these findings, they proposed a novel mechanism for the generation of Aβ via autophagy that emphasized the prominent role of autophagy in AD pathogenesis.[41]

PD is a neurodegenerative disorder associated with progressive loss of dopaminergic neurons of the substantia nigra and locus coeruleus. The major clinical symptoms of PD are body rigidity, hypokinesia, and postural instability associated with trembling extremities.[42] Pathological examination shows marked accumulation of cytoplasmic inclusions of proteinaceous material with lipids called Lewy bodies. Lewy bodies consist of lipids, ubiquitin, enzymes involved in ubiquitin-related pathways, neurofilament proteins, α-synuclein, synphilin-1, and other entangled proteins. Mutations in the gene encoding α-synuclein, which is localized in presynaptic terminals and is abundantly present in Lewy bodies, are identified in certain cases of familial PD.[43,44] α-Synuclein is a protein of unknown function and a major component of Lewy bodies. Among three point mutations in α-synuclein causing an autosomal dominant form of familial PD, two mutations of α-synuclein (A53T and A30P) have been studied extensively. These α-synuclein mutants have a stronger tendency to form fibrils than wild-type α-synuclein. Hence, similar to huntingtin with abnormal polyQ expansion, misfolded or aggregated α-synuclein is believed to cause cell toxicity and inhibits the ubiquitin-proteasome system. Lewy bodies may contribute to aggregation of α-synuclein into inclusions to moderate its toxicity.[45,46] It has been reported recently that autophagic-lysosomal dysfunction may be also involved in PD. Using stable PC12 transfectants expressing wild-type and A53T mutant α-synuclein, Stefanis *et al.*[47] showed that marked accumulation of autophagic vacuoles and impairment of lysosomal and ubiquitin-proteasome functions are principal phenotypes in the cells. On the other hand, clearance of mutant α-synuclein is strongly dependent on both ubiquitin-proteasomes and macroautophagy,[48] but not chaperone-mediated autophagy capable of degrading wild-type α-synuclein efficiently.[49]

Impairment of Autophagy in Neurons

Recently, our group and Mizushima's group investigated the pathophysiological roles of basal or constitutive autophagy in the brain.[50,51] For this purpose, we generated neuron-specific autophagy-deficient mice (*Atg7*$^{F/F}$:Nes mice) by crossing *Atg7*-conditional knockout mice (*Atg7*$^{F/F}$) with transgenic mice expressing the Cre recombinase under the control of the neuron-specific Nestin (Nes) promoter, Nes-*Cre*. We found that mice lacking Atg7 (i.e., autophagy) in the central nervous system exhibited various behavioral deficits, such as abnormal limb-clasping reflexes and reduction of coordinated movement, and died within 28 weeks after birth. Histological analysis showed that *Atg7*-deficiency was associated with neuronal loss in the cerebral and cerebellar cortices. Intriguingly, *Atg7*-deficient neurons showed abundant accumulation of polyubiquitylated proteins, which appeared as inclusion bodies whose size and number increased with aging (Figure 3), but had functionally intact proteasomes, whose impairment is generally known to cause abnormal ubiquitin-mediated proteolysis.[50] Hara *et al*.[51] also reported that almost all these phenotypes, if not all, were observed in neural-specific mice deficient in *Atg5*, another autophagy-essential gene. Thus, many of the critical symptoms seen in neural-specific autophagy-deficient mice are similar to those of patients with neurodegenerative disorders.

Histological analyses of the brains of *Atg7*$^{F/F}$:Nes mice revealed loss of specific neurons, such as pyramidal neurons in the cerebral cortex and hippocampus, and Purkinje cells in the cerebellum. Unexpectedly, immunohistological analysis using anti-ubiquitin antibody identified ubiquitin-positive proteinaceous aggregates throughout the brain, although the staining intensity varied from one region to another. Few ubiquitin-positive inclusions were recognized in brain regions with evident neuronal loss, whereas many ubiquitin inclusions were noted in areas with barely any neuronal loss such as the hypothalamus. Although we could not determine whether neuronal death is due to accumulation and subsequent inclusion formation of ubiquitylated proteins, neurons with large inclusions survived. Conversely, large pyramidal neurons and Purkinje cells seem vulnerable to ubiquitylated proteins and die before the formation of large inclusions. Whether the formation of inclusion bodies in neurons is protective or toxic is under debate, although emerging evidence emphasizes that protein aggregation can be a protective mechanism.[32,33]

Although accumulation of ubiquitylated proteins and cell death were noted in autophagy-deficient hepatocytes[14] and neurons,[50,51] such phenotypes were not observed in growing cells such as mouse embryonic fibroblasts (MEFs) and astroglial cells, irrespective of autophagy deficiency. Thus, it seems that autophagy is not required in rapidly dividing cells, at least with respect to multiplication of these cells. These results might also reflect the difference in autophagic activity among cell types. It is possible that the cell division cycle results in dilution of ubiquitylated proteins in autophagy-deficient MEFs, preventing their accumulation. Alternatively, other degradation pathways, such as chaperone-mediated autophagy, could contribute to degradation of long-lived proteins in growing MEFs. Considered together, it is clear that macroautophagy (the massive autophagy pathway discussed here) plays important roles in proteolysis in quiescent cells.

Autophagy deficiency is considered to result in delays of global turnover of cytoplasmic components, resulting in accumulation of misfolded and/or unfolded proteins followed by formation of inclusion bodies. However, a recent report showed that p62/SQSTM1 harboring a ubiquitin binding domain, interacted with LC3 and was degraded via autophagy.[52] We also obtained similar results and found that

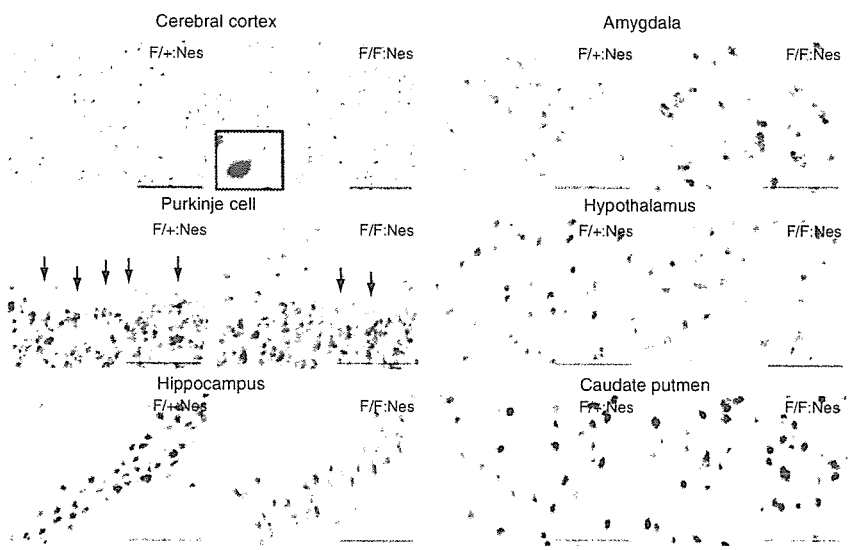

Figure 3 Ubiquitin-positive inclusions in autophagy-deficient neurons. The presence of ubiquitin-positive dots was examined immunohistochemically in several regions of the brain including cerebral cortex, cerebellum (Purkinje cells), hippocampus, amygdala, hypothalamus, caudate putamen of *Atg7*$^{F/+}$:Nes (left panels), and *Atg7*$^{F/F}$:Nes (right panels) mice. Note the presence of numerous ubiquitin dots in the amygdala and hypothalamus of representative mutants. Bars, 100 μm in the panel of cerebral cortex, and 50 μm in others